Mechanics of Materials 42 (2010) 451–468

Contents lists available at ScienceDirect

Mechanics of Materials

journal homepage: www.elsevier.com/locate/mechmat

Macroscopic response and stability in lamellar nanostructured elastomers with "oriented" and "unoriented" polydomain microstructures

Vikranth Racherla [a,1], Oscar Lopez-Pamies [b], Pedro Ponte Castañeda [c,*]

[a] Laboratoire de Mécanique des Solides, École Polytechnique, 91128 Palaiseau, France
[b] Department of Mechanical Engineering, State University of New York, Stony Brook, NY 11794-2300, USA
[c] Department of Mechanical Engineering and Applied Mechanics, University of Pennsylvania, Philadelphia, PA 19104-6315, USA

ARTICLE INFO

Article history:
Received 27 July 2009
Received in revised form 2 November 2009

Keywords:
Lamellar TPEs
Homogenization
Microstructure evolution
Macroscopic instabilities

ABSTRACT

We propose a homogenization-based framework to construct constitutive models for the macroscopic response of polycrystalline hyperelastic solids. The theory is presented in a rather general context, but attention is primarily focused on its specialization to lamellar thermoplastic elastomers (TPEs). The proposed framework incorporates direct information on the constitutive properties of the soft and hard blocks, the lamellar nanostructure, as well as the complete orientation distribution (i.e., the lamination directions) and average shape of the grains. In addition to providing constitutive models for the macroscopic response of lamellar TPEs, the proposed theory also provides information about the evolution of the underlying nano- and micro-structure – including the crystallographic texture – and the associated development of macroscopic instabilities. It is found that for sufficiently large stiffness contrast (between the hard and soft blocks) and sufficiently high Poisson's ratio of the soft blocks there is a sudden change in the deformation mode of "unfavorably" oriented (perpendicular to the tensile direction) layers – from a high-energy triaxial deformation mode to a lower-energy rotation and shear-along-the-layers mode, which is responsible for a reduction in the overall stiffness of the granular aggregate. This reduction in stiffness can lead to the development of shear-band-type instabilities, which are perpendicular to the "unfavorably" oriented layers, and may be precursors to the chevron-type instabilities that have been observed in these material systems. The effect of the constitutive properties of the blocks and of the initial microstructure on the overall behavior, microstructure evolution and the possible development of these elastic instabilities is investigated in some detail.

1. Introduction

TPEs (thermoplastic elastomers) are a technologically important class of multiphase polymers consisting of macromolecular chains with alternating hard and soft blocks. Due to chemical incompatibility, the hard and soft blocks self-separate during processing to form distinct morphologies at the *nano*-scale. These include, depending on the volume fractions of hard and soft blocks, periodic arrangements of lamellae, hexagonally packed rods, and body-centered cubic arrays of spheres of one phase embedded in the other (see, e.g., Fredrickson and Bates, 1996). These nanomorphologies, however, need not be globally aligned. In particular, TPEs exhibit a granular structure at the *micron* level, much like metal polycrystals, with different grains exhibiting different alignment directions. (Some classes of semi-crystalline polymers exhibit this type of dual

* Corresponding author.
E-mail addresses: vikranth.racherla@mech.iitkgp.ernet.in (V. Racherla), oscar.lopez-pamies@sunysb.edu (O. Lopez-Pamies), ponte@seas.upenn.edu (P. Ponte Castañeda).
[1] Present address: Department of Mechanical Engineering, Indian Institute of Technology, Kharagpur 721302, India.

0167-6636/$ - see front matter © 2009 Elsevier Ltd. All rights reserved.
doi:10.1016/j.mechmat.2009.11.005

microstructure as well.) Precisely what type of global alignment can be found in TPEs depends greatly on the processing technique employed to make them. While it is straightforward to generate a random and isotropic distribution of domain orientations leading to "unoriented" TPEs (see, e.g., Gido et al., 1993), it is more challenging (see, e.g., Honeker and Thomas, 1996) to generate a highly textured distribution of domains leading to "oriented" TPEs.

The soft phase in TPEs, at room temperature and quasi-static loading conditions, is generally isotropic and can undergo large reversible (elastic) deformations with little hysteresis. On the other hand, the hard phase typically exhibits an initially stiff, elastic response followed by plastic yielding with significant hysteresis, or brittle fracture. These generic properties of the phases simply arise from the fact that while the glass transition (or melting) temperature of the soft phase is lower than room temperature, the corresponding glass transition (or melting) temperature of the hard phase is much higher.

The ability to tailor macroscopic properties – including elastic stiffness, fracture toughness, and stretchability – by simply varying the proportions of the hard and soft blocks and the crystallographic texture, combined with superior processability characteristics, has lead to the increasing usage of TPEs in place of standard vulcanized elastomers. In addition, TPEs have also demonstrated considerable potential for utilization in a wide variety of emerging technologies, including high-density electronic storage devices (Cheng et al., 2001), filtration membranes for viruses (Yang et al., 2006) and antireflection coatings (Joo et al., 2006). It is plain that the development of constitutive models incorporating detailed information on the underlying nanomorphologies, crystallographic texture, and the constitutive properties of the hard and soft blocks is of the essence for the successful implementation of TPEs in such advanced applications.

Previous theoretical efforts to study TPEs taking into account the underlying microstructure have been mainly devoted to *perfectly oriented* TPEs with lamellar structure. For instance, Allan et al. (1991) studied the small-strain, linear-elastic response of oriented lamellar styrene-butadiene-styrene (SBS) triblock copolymers, arguably the most commercially utilized TPE, by modeling these material systems as perfect laminates. In a later contribution, Read et al. (1999) carried out a combined theoretical and finite-element analysis of the behavior of two-dimensional (2D) perfectly oriented TPEs, subjected to tensile loading perpendicular to the lamellae, focusing on the possible buckling of the layers and its connection with the development of "chevron" patterns. Unlike Allan et al. (1991), Read et al. (1999) did take into account the finite rotations of the layers, although only approximately. They found that for perfectly oriented TPEs there is a geometric instability that leads to a sharp turnover in the macroscopic stress-strain response due to the microscopic formation of "chevron patterns". This geometric instability occurs even when the phases are taken to be purely elastic; the plastic behavior of the hard phase only tends to accentuate the post-bifurcated chevron profile. Motivated by the experimental findings of Cohen et al. (2000), Tzianetopoulou and Boyce (2004) conducted plane-strain numerical simulations for the mechanical response of oriented TPEs subjected to large deformations normal and parallel to the lamellae, accounting for lamellar waviness and interface/interphase imperfections, as well as the effect of clay nano-particles. In addition in her Ph.D. thesis, Tzianetopoulou (2007) proposed an analytical continuum constitutive model for 2D hyperelastic laminates composed of compressible Neo-Hookean phases, and used this model in 2D finite elements calculations to explore the behavior of polycrystalline TPEs.

In the context of the above-mentioned work for perfectly oriented TPEs, it is relevant to remark that geometrically driven instabilities for layered media have been theoretically examined in the more general framework of finite elasticity by Triantafyllidis and co-workers (Triantafyllidis and Maker, 1985; Geymonat et al., 1993; Triantafyllidis and Nestorvić, 2005). These works aimed to determine all possible (elastic) instabilities in such materials, including long-wavelength instabilities, which correspond to loss of strong ellipticity of the resulting macroscopic response. In addition, a general constitutive model for the response of hyperelastic layered materials under finite deformations – including exact relations for the rotation of the layers – has been developed by Lopez-Pamies and Ponte Castañeda (2009) (see also Lopez-Pamies (2006)). In that work, the possible development of long-wavelength, or "macroscopic" instabilities was found to be intimately related to the rotation of the layers under finite-strain loading conditions.

More recently, Lopez-Pamies et al. (2008) have proposed a methodology for modeling highly, but imperfectly oriented lamellar TPEs as "polycrystalline" aggregates of grains consisting of perfect laminates with slightly different orientations, whose macroscopic properties can be computed via a two-scale homogenization process. This constitutive framework accounts for finite deformations, and in addition to providing the macroscopic stress-strain response of TPEs, it also allows monitoring of the evolution of the underlying nano-morphologies and crystallographic texture, as well as detecting the onset of macroscopic instabilities. In their study, these authors worked out results for highly oriented TPEs made up of *two* families of grains with slightly different lamination orientations, and found that the rotation of the layers within the grains is a key deformation mechanism controlling the macroscopic response and stability of lamellar TPEs.

In this paper, we extend the framework of Lopez-Pamies et al. (2008) to model lamellar TPEs with completely general crystallographic texture (as opposed to only two families of grains); particular attention is given to the case of two-phase lamellar TPEs with ellipsoidal grain shapes. Thus, the primary aim of this work is to develop tools for generating constitutive models describing the macroscopic response of lamellar TPEs. For the first time, such models simultaneously take into account direct information on the properties of the underlying hard and soft blocks, the lamellar nanomorphology, and the complete orientation distribution of the grains at the micron level. However, it is important to emphasize that the work is directly relevant to TPEs with other types of domain structures, as well as for other types of nanostructured polymeric systems, such as semi-crystalline polymers (e.g., Lee et al., 1993;

Krumova et al., 2006; Nikolov et al., 2006). Three important assumptions are made in the proposed analysis. First, separation of length scales is assumed at the single-crystal and polycrystalline levels, allowing the homogenization of the individual grains and of the polycrystalline specimen to be performed in two successive steps. Second, neglecting strain-rate and hysteresis effects (and assuming "proportional" or nearly proportional loading in the hard phase), the hard and soft phases are characterized by hyperelastic stored-energy functions. Finally, building on the works of Read et al. (1999) and Lopez-Pamies et al. (2008), plastic deformation is essentially neglected and loss of strong ellipticity (LSE) of the macroscopic response of the homogenized specimen is used to estimate the possible development of macroscopic elastic instabilities. Plastically driven instabilities may occur earlier, depending on the loading conditions, but a careful treatment of these instabilities is beyond the scope of this work, in which we will be satisfied with crude estimates for when plastic deformation may start to become important.

The paper is organized as follows. In Section 2, we introduce some basic notation and define the homogenized (macroscopic) response and stability of a fairly general class of hyperelastic polycrystals. In Section 3, we specialize the formulation of Section 2 to the case of lamellar TPEs and carry out the appropriate computations. More specifically, Section 3.1 deals with the computation of the effective behavior of the individual grains, which are made up of perfect laminates with alternating layers of hard and soft phases. Sections 3.2 and 3.3 spell out the calculation – based on the tangent second-order (TSO) method (Ponte Castañeda, 1996; Ponte Castañeda and Willis, 1999; Ponte Castañeda and Tiberio, 2000) – of the macroscopic response of the polycrystal. In Section 3.4, we identify a set of microstructural variables whose evolution along a finite-deformation loading path help reveal geometric mechanisms that have a major effect on the macroscopic response of TPEs. Section 4 presents an application of the constitutive framework put forward in Section 3 for a model class of TPEs with unoriented (Section 4.1) and oriented (Section 4.2) crystallographic textures. A detailed study of the macroscopic response, onset of macroscopic instabilities, onset of yielding of the hard phase, and evolution of microstructure, as functions of the properties of the hard and soft phases is provided for these two cases. We conclude the paper in Section 5 with some theoretical and practical remarks.

2. Hyperelastic polycrystals: microstructure description and overall behavior

Consider a statistically uniform polycrystalline specimen occupying a domain Ω_0, with boundary $\partial\Omega_0$, in the reference configuration.[2] It is assumed that there are N different crystal orientations characterized by proper orthogonal tensors $\mathbf{Q}_0^{(r)}$ $(r = 1, \ldots, N)$ relative to a given reference crystal orientation, and that all the crystals (or grains) are perfectly bonded. Furthermore, the crystals are anisotropic hyperelastic solids, homogeneous at a length scale of the order of the grain size, that are characterized by non-convex stored-energy functions

$$W^{(r)}(\mathbf{F}) = W_c(\mathbf{F}\mathbf{Q}_0^{(r)T}), \quad r = 1, \ldots, N. \tag{1}$$

Here, W_c is the stored-energy function of the reference crystal and $\mathbf{F}(\mathbf{X}) = \partial\mathbf{x}/\partial\mathbf{X}$ (with $\mathbf{x}$, $\mathbf{X}$ denoting, respectively, the positions of the same material point in deformed and undeformed configurations) is the deformation gradient tensor. The anisotropic potential for the reference crystal is, of course, taken to be objective so that

$$W_c(\mathbf{F}) = W_c(\mathbf{Q}\mathbf{F}), \tag{2}$$

for all proper orthogonal tensors $\mathbf{Q}$ and all deformation gradients $\mathbf{F}$. In addition, for consistency with the classical theory of linear elasticity

$$W_c(\mathbf{F}) = \frac{1}{2}\boldsymbol{\varepsilon}\cdot\mathscr{L}_c\boldsymbol{\varepsilon} + O(||\mathbf{F}-\mathbf{I}||^3) \tag{3}$$

in the limit of small deformations as $\mathbf{F}\to\mathbf{I}$. In the above expression, $\boldsymbol{\varepsilon} = (\mathbf{F}+\mathbf{F}^T-2\mathbf{I})/2$ is the infinitesimal strain tensor, and $\mathscr{L}_c$ is a *positive definite* fourth-order modulus tensor. Thus, in view of (3), W_c is strongly elliptic for sufficiently small deformations, but may lose strong ellipticity at larger deformations.

The initial microstructure, i.e., the initial distribution of crystal orientations within the specimen, is characterized by indicator functions

$$\chi_0^{(r)}(\mathbf{X}) = 1 \text{ if } \mathbf{X}\in\Omega_0^{(r)} \quad \text{and } 0 \text{ otherwise}, \tag{4}$$

where $\Omega_0^{(r)}\subseteq\Omega_0$ is the subdomain occupied by crystals with orientation tensor $\mathbf{Q}_0^{(r)}$. In practice, however, the complete microstructural information embodied in the indicator functions is usually not accessible experimentally. Instead, only certain microstructural features, such as the n-point probabilities, are available. In this work we make use of the one-point probability function, $p_0^{(r)}(\mathbf{X})$, denoting the probability of finding phase r at $\mathbf{X}$, and of the two-point probability function, $p_0^{(rs)}(\mathbf{X},\mathbf{X}')$, denoting the probability of finding phase r at $\mathbf{X}$ and phase s at $\mathbf{X}'$ simultaneously. In particular, assuming ergodicity of the specimen and "ellipsoidal symmetry" (Willis, 1977) with no-long range order for the two-point statistics, the initial one- and two-point probabilities of the microstructure are given by

$$\begin{aligned} &p_0^{(r)}(\mathbf{X}) = c_0^{(r)} \quad \text{and} \\ &p_0^{(rs)}(\mathbf{X},\mathbf{X}') = p_0^{(rs)}(|\mathbf{Z}_0^T(\mathbf{X}'-\mathbf{X})|) \quad \text{with} \\ &p_0^{(rs)}\to 0 \text{ as} |\mathbf{X}'-\mathbf{X}|\to\infty, \end{aligned} \tag{5}$$

where $c_0^{(r)}$ are the volume fractions of crystals with orientations $\mathbf{Q}_0^{(r)}$, and $\mathbf{Z}_0$ is a second-order shape tensor serving to characterize the average shape of the grains.

It should also be pointed out that the polycrystalline texture or the one-point statistics for the specimen, in the undeformed configuration, is often specified via the orientation distribution function (ODF) p_0 (α_k) which gives the probability of finding crystals as a function of orientation (e.g., Euler or Rodrigues) parameters α_k. More specifically, if $\mathscr{F}$ denotes the domain of orientation parameters α_k

[2] From here on, the subscript 0 shall refer to variables in the undeformed reference configuration.

for which there is a one-to-one and onto mapping from $\mathscr{F}$ to the set of all distinct crystal orientations $\mathscr{C}$, the initial ODF $p_0\ (\alpha_k)$ is defined such that the volume fraction c_0 of grains with orientations in subdomain $\mathscr{G} \subseteq \mathscr{F}$ is given by

$$c_0 = \int_{\mathscr{G}} p_0\ (\alpha_k)\ d\mu, \quad \text{with} \quad \int_{\mathscr{F}} p_0(\alpha_k)\ d\mu = 1, \tag{6}$$

where $d\mu$ is the appropriate measure associated with an infinitesimal element in $\mathscr{F}$. It is also useful to note that $\mathscr{F}$ can be one-, two-, or three-dimensional depending on the nature of crystal symmetries. Correlation functions can also be defined to specify two-point statistics (see Adams and Olson (1998) for details, as well as for relations between the orientation parameters α_k and the orientation tensor $\mathbf{Q}$). However, this will not be needed in this work, since the approach adopted here only makes use of the second-order shape tensor $\mathbf{Z}_0$. More specifically, when the two-point statistics are assumed to exhibit the form defined in Eq. (5), their exact functional form (i.e., the radial dependence) does not influence the macroscopic behavior of the specimen. It should finally be mentioned that we make use of both discrete as well as continuous representations of texture. While the discrete representation of one-point statistics in the undeformed configuration is used for computing the overall behavior of the specimen as a function of initial microstructure, the continuous representation, provided by the ODF, is used for graphical illustration of the evolution of the microstructure and for specifying the initial one-point statistics.

Having defined the constitutive behavior of the crystals and the initial microstructure, the local constitutive equation, relating the deformation gradient and the first-Piola Kirchhoff stress $\mathbf{S}(\mathbf{X})$, can be written as

$$\mathbf{S} = \frac{\partial W}{\partial \mathbf{F}}(\mathbf{X}, \mathbf{F}), \quad W(\mathbf{X}, \mathbf{F}) = \sum_{r=1}^{N} \chi_0^{(r)}(\mathbf{X}) W^{(r)}(\mathbf{F}). \tag{7}$$

Under the hypothesis that the specimen size is much larger than the typical grain size, following Hill (1972), the macroscopic constitutive equation for the hyperelastic polycrystal relating the average stress $\overline{\mathbf{S}} = \langle \mathbf{S} \rangle$ to the average deformation $\overline{\mathbf{F}} = \langle \mathbf{F} \rangle$ is then given by

$$\overline{\mathbf{S}} = \frac{\partial \widetilde{W}}{\partial \overline{\mathbf{F}}}(\overline{\mathbf{F}}), \quad \widetilde{W}(\overline{\mathbf{F}}) = \min_{\mathbf{F}(\mathbf{X}) \in \mathscr{K}(\overline{\mathbf{F}})} \langle\ W(\mathbf{X}, \mathbf{F})\ \rangle, \tag{8}$$

where angular brackets $\langle \cdot \rangle$ denote volume average over Ω_0, $\widetilde{W}(\overline{\mathbf{F}})$ denotes the effective (average) stored-energy function, and $\mathscr{K}$ denotes the set of admissible deformation gradients satisfying affine displacement boundary conditions $\mathbf{x} = \overline{\mathbf{F}}\mathbf{X}$ on $\partial\Omega_0$, i.e.,

$$\mathscr{K}(\overline{\mathbf{F}}) = \Big\{ \mathbf{F} \mid \exists\ \mathbf{x} = \mathbf{x}(\mathbf{X}) \quad \text{with} \quad \mathbf{F} = \frac{\partial \mathbf{x}}{\partial \mathbf{X}}, \\ J = \det(\mathbf{F}) > 0 \quad \text{in} \quad \Omega_0, \ \mathbf{x} = \overline{\mathbf{F}}\mathbf{X} \quad \text{on} \quad \partial\Omega_0 \Big\} \tag{9}$$

Thus, while the stored-energy functions $W^{(r)}$ describe the local (microscopic) behavior and the indicator functions $\chi_0^{(r)}$ describe the initial microstructure, the effective stored-energy function $\widetilde{W}$ computed via the minimum variational statement (8) characterizes the macroscopic behavior of the polycrystal.

The *minimum* problem (8) is extremely difficult to solve for several reasons including the lack of convexity of the local stored-energy functions $W^{(r)}$, as well as the unavailability of complete information on the underlying microstructure $\chi_0^{(r)}$. Therefore, following the work of Lopez-Pamies and Ponte Castañeda (2006) and Michel et al. (2007) (see Section 2 in these references), the effective potential for the polycrystal is instead determined via the associated *stationary* variational problem from which the macroscopic constitutive equation is approximated as

$$\overline{\mathbf{S}} = \frac{\partial \widehat{W}}{\partial \overline{\mathbf{F}}}(\overline{\mathbf{F}}), \quad \widehat{W}(\overline{\mathbf{F}}) = \underset{\mathbf{F}(\mathbf{X}) \in \mathscr{K}(\overline{\mathbf{F}})}{\text{stat}} \langle W(\mathbf{X}, \mathbf{F}) \rangle. \tag{10}$$

Here, the stationary operation formally indicates the selection of the "principal solution" of the Euler-Lagrange equations associated with the variational principle (8), without worrying whether it is the actual minimizing solution. In essence, the definition (10) ignores the possible development of bifurcated solutions associated with local instabilities. It does contain, however, information about the onset of "macroscopic" instabilities with wavelengths comparable to the specimen dimensions (Geymonat et al., 1993), as signaled by its loss of strong ellipticity (LSE):

$$\widehat{B}(\overline{\mathbf{F}}) = \min_{|\mathbf{u}|=|\mathbf{V}|=1} \left\{ u_i V_j \widehat{\mathscr{L}}_{ijkl}(\overline{\mathbf{F}}) u_k V_l \right\} > 0, \tag{11}$$

where

$$\widehat{\mathscr{L}}_{ijkl}(\overline{\mathbf{F}}) = \frac{\partial^2 \widehat{W}}{\partial F_{ij} \partial F_{kl}}(\overline{\mathbf{F}}). \tag{12}$$

Note that loss of strong ellipticity, as detected from failure of condition (11), provides the critical deformation gradients, $\overline{\mathbf{F}}_{cr}$, at which the homogenized material becomes macroscopically unstable, as well as the pairs of unit vectors $\mathbf{V}$ and $\mathbf{u}$ for which these macroscopic instabilities occur. Here, $\mathbf{V}$ denotes the normal (in the undeformed configuration) to the surface of a weak or strong discontinuity of the deformation field, whereas $\mathbf{u}$ characterizes the type of deformation associated with such a discontinuity (see, e.g., Knowles and Sternberg, 1975).

3. Application to lamellar TPEs

As already stated in Section 1, lamellar TPEs are considered here as a two-scale material system made up of a polycrystalline aggregate of single crystals, which in turn are made up of laminates of the hard and soft phases. In this section, we employ the general formulation of Section 2 for hyperelastic polycrystals to construct a constitutive model for such a class of TPEs. First, in Section 3.1, we formulate and solve the problem for the effective potentials $W^{(r)}$ of the individual grains. Having determined the behavior of the crystals, we then put forward in Section 3.2, by means of the tangent second-order variational method, an estimate for the effective stored-energy function (10) of the resulting polycrystal. Section 3.3 spells out the expressions for the average deformation gradients in an auxiliary linear comparison composite (LCC) that are central to the computation of the tangent second-order approximation of $\widehat{W}$. Finally, in Section 3.4, we write down formulae for

the evolution of microstructural variables that are particularly helpful in revealing the main microscopic deformation mechanisms governing the macroscopic response of lamellar TPEs.

3.1. Lamellar single crystals: microstructure and effective behavior

In this work, the single crystals that make up the polycrystalline structure of lamellar TPEs are taken to be perfect laminates composed of a "soft" phase with stored-energy function $W_c^{(1)}$ and a "hard" phase with stored-energy function $W_c^{(2)}$ in initial volume fractions f_0 and $1-f_0$, respectively. Assuming piecewise constant fields in the phases, the effective potential W_c for the reference single crystal can be shown to be of the form (see, e.g., Triantafyllidis and Maker, 1985; Lopez-Pamies and Ponte Castañeda, 2009)

$$W_c(\mathbf{F}) = f_0 W_c^{(1)}(\mathbf{F}_s) + (1-f_0) W_c^{(2)}(\mathbf{F}_h), \tag{13}$$

where, based on the compatibility requirement, the deformation gradients in the soft and hard phases are, respectively, of the form

$$\mathbf{F}_s = \mathbf{F} + (1-f_0)\boldsymbol{a}\otimes\mathbf{N} \quad \text{and} \quad \mathbf{F}_h = \mathbf{F} - f_0\boldsymbol{a}\otimes\mathbf{N}, \tag{14}$$

with $\mathbf{N}$ denoting the initial lamination direction for the reference single crystal. The vector $\boldsymbol{a}$ in (14) is determined by the equilibrium condition

$$\left[\frac{\partial W_c^{(1)}}{\partial \mathbf{F}}(\mathbf{F}_s) - \frac{\partial W_c^{(2)}}{\partial \mathbf{F}}(\mathbf{F}_h)\right]\mathbf{N} = 0. \tag{15}$$

Note that by assuming piecewise constant fields, we are indeed following the "principal solution" to the variational problem associated with computation of effective potential W_c. However, this may not correspond to the lowest energy solution, particularly at large deformations, when local instabilities may take place. Thus, within the framework adopted here, we are implicitly assuming that local instabilities in the grains, which might occur for certain special grain orientations, do not significantly affect the macroscopic response and stability of the polycrystal.

For later use in the computation of the approximation for $\widehat{W}$, it is useful to note that (see Lopez-Pamies and Ponte Castañeda (2009) and deBotton and Ponte Castañeda (1992) for analogous problems in plasticity)

$$\frac{\partial W_c}{\partial \mathbf{F}}(\mathbf{F}) = f_0\ \frac{\partial W_c^{(1)}}{\partial \mathbf{F}}(\mathbf{F}_s) + (1-f_0)\frac{\partial W_c^{(2)}}{\partial \mathbf{F}}(\mathbf{F}_h), \tag{16}$$

and

$$\frac{\partial^2 W_c}{\partial \mathbf{F}\partial \mathbf{F}}(\mathbf{F}) = f_0\ \mathbb{L}_c^{(1)} + (1-f_0)\ \mathbb{L}_c^{(2)}\left[\mathbb{I} + \mathbb{P}_c^{(1)}(\mathbb{L}_c^{(2)} - \mathbb{L}_c^{(1)})\right], \tag{17}$$

where

$$\mathbb{L}_c^{(1)} = \frac{\partial^2 W_c^{(1)}}{\partial \mathbf{F}\partial \mathbf{F}}(\mathbf{F}_s), \quad \text{and} \quad \mathbb{L}_c^{(2)} = \frac{\partial^2 W_c^{(2)}}{\partial \mathbf{F}\partial \mathbf{F}}(\mathbf{F}_h) \tag{18}$$

are the incremental modulus tensors of the soft and hard phases, respectively, $\mathbb{I}$ is the fourth-order identity tensor with Cartesian components $I_{ijkl} = \delta_{ik}\delta_{jl}$, and $\mathbb{P}_c^{(1)}$ is the relevant fourth-order microstructural tensor for layered microstructures with Cartesian components given by $P_{c\ ijkl}^{(1)} = (L_{c\ ipkq}^{(1)} N_p N_q)^{-1} N_j N_l$.

3.2. Variational approximation for $\widehat{W}$

Having defined the constitutive potentials for the lamellar single crystals, we now work out an approximation for the effective potential $\widehat{W}$ of the resulting polycrystal, as defined by $(10)_2$. This is accomplished here by making use of the tangent second-order (TSO) variational procedure of Ponte Castañeda and Tiberio (2000). Thus, the TSO approximation for the effective potential $\widehat{W}$ is given by

$$\widehat{W}(\overline{\mathbf{F}}) = \sum_{r=1}^{N}\left[W^{(r)}(\overline{\mathbf{F}}_l^{(r)}) + \frac{1}{2}\frac{\partial W^{(r)}}{\partial \mathbf{F}}(\overline{\mathbf{F}}_l^{(r)})\cdot(\overline{\mathbf{F}} - \overline{\mathbf{F}}_l^{(r)})\right], \tag{19}$$

where $\overline{\mathbf{F}}_l^{(r)}$ is the average deformation gradient in phase r of an N-phase linear comparison composite (LCC) with the same initial microstructure that is subjected to the same affine displacement boundary conditions as the hyperelastic polycrystal. The behavior of the phases of the LCC is characterized by quadratic potentials of the form

$$W_l^{(r)}(\mathbf{F}) = \frac{1}{2}(\mathbf{F}-\mathbf{I})\cdot\mathbb{L}^{(r)}(\mathbf{F}-\mathbf{I}) + \mathbf{T}^{(r)}\cdot(\mathbf{F}-\mathbf{I}) + f^{(r)}, \tag{20}$$

where $\mathbf{I}$ is the second-order identity tensor and

$$\begin{aligned}
&\mathbb{L}^{(r)} = \frac{\partial^2 W^{(r)}}{\partial \mathbf{F}\partial \mathbf{F}}\left(\overline{\mathbf{F}}_l^{(r)}\right),\\
&\mathbf{T}^{(r)} = \mathbb{L}^{(r)}\left(\mathbf{I} - \overline{\mathbf{F}}_l^{(r)}\right) + \frac{\partial W^{(r)}}{\partial \mathbf{F}}\left(\overline{\mathbf{F}}_l^{(r)}\right), \text{ and}\\
&f^{(r)} = \frac{1}{2}\left(\mathbf{I} - \overline{\mathbf{F}}_l^{(r)}\right)\cdot\mathbb{L}^{(r)}\left(\mathbf{I} - \overline{\mathbf{F}}_l^{(r)}\right) + \frac{\partial W^{(r)}}{\partial \mathbf{F}}\left(\overline{\mathbf{F}}_l^{(r)}\right)\cdot\left(\mathbf{I} - \overline{\mathbf{F}}_l^{(r)}\right) + W^{(r)}\left(\overline{\mathbf{F}}_l^{(r)}\right).
\end{aligned} \tag{21}$$

Note that the TSO estimate (19) for the effective stored-energy function of the hyperelastic polycrystal $(10)_2$ reduces ultimately to the computation of the phase averages of the deformation gradient field in the above-defined LCC, which is a reasonably simple task in view of the *linearity* of this problem. Indeed, the estimation of the phase averages of the fields in linear-elastic media is standard and several homogenization methods have been devised for this purpose (see, e.g., Milton, 2002). The above-defined linear comparison problem is not a standard problem in linear elasticity – because of the non-symmetry of the stress and strain measures – but it is linear nonetheless and the methods that have been developed for classical linear elasticity are equally applicable to these more general linear materials (see, e.g., Ponte Castañeda and Tiberio, 2000).

3.3. Phase averages of the deformation gradient in the LCC

Next, we present the linear homogenization scheme for computing the phases averages of the deformation gradient in the LCC, needed for the computation of the TSO approximation (19) for $\widehat{W}$. By treating the LCC as a linear thermoelastic composite, and generalizing appropriately the work of Laws (1973), the phase averages of the deformation gradients can be shown to be of the form.

$$\overline{\mathbf{F}}_l^{(r)} = \mathbb{A}^{(r)}(\overline{\mathbf{F}} - \mathbf{I}) + \boldsymbol{a}^{(r)} + \mathbf{I}, \tag{22}$$

where the quantity $\overline{\mathbf{F}} - \mathbf{I}$ now plays the role of the infinitesimal strain in the usual calculation. In these expressions,

$\mathbb{A}^{(r)}$ and $\boldsymbol{a}^{(r)}$ are fourth- and second-order "strain" concentration tensors, respectively, depending on the microstructure and elastic moduli of the constituents in the LCC. The concentration tensor $\mathbb{A}^{(r)}$ has major symmetry ($A^{(r)}_{ijkl} = A^{(r)}_{klij}$), but not minor symmetry ($A^{(r)}_{ijkl} \neq A^{(r)}_{jikl}$). In addition, from the fact that for affine displacement boundary conditions $\langle \mathbf{F}_l \rangle = \overline{\mathbf{F}}$, we have that the concentration tensors must satisfy

$$\sum_{r=1}^{N} c_0^{(r)} \mathbb{A}^{(r)} = \mathbb{I} \quad \text{and} \quad \sum_{r=1}^{N} c_0^{(r)} \boldsymbol{a}^{(r)} = 0. \tag{23}$$

For linear polycrystals with "ellipsoidal" microstructures, as defined by relations (5) for the one- and two-point probability functions, self-consistent estimates for the concentration tensors, generalizing those of Laws (1973) and Willis (1977, 1981), may be obtained as

$$\begin{aligned} \mathbb{A}^{(r)} &= \left[\mathbb{I} + \widetilde{\mathbb{P}}(\mathbb{L}^{(r)} - \widetilde{\mathbb{L}})\right]^{-1} \\ \boldsymbol{a}^{(r)} &= \mathbb{A}^{(r)} \widetilde{\mathbb{P}} \left[\sum_{s=1}^{N} c_0^{(s)} \mathbf{T}^{(s)} \mathbb{A}^{(s)} - \mathbf{T}^{(r)}\right], \end{aligned} \tag{24}$$

where $\mathbb{L}^{(r)}, \mathbf{T}^{(r)}$ have been defined in the previous subsection and $\widetilde{\mathbb{L}}$ is the effective modulus tensor satisfying the implicit equation:

$$\widetilde{\mathbb{L}} = \sum_{r=1}^{N} c_0^{(r)} \mathbb{L}^{(r)} \left[\mathbb{I} + \widetilde{\mathbb{P}}(\mathbb{L}^{(r)} - \widetilde{\mathbb{L}})\right]^{-1}. \tag{25}$$

In the above expressions, $\widetilde{\mathbb{P}}$ is a microstructural tensor, which for the class of "ellipsoidal" microstructures considered here, may be expressed (Willis, 1977) as

$$\widetilde{\mathbb{P}} = \frac{1}{4\pi \det \mathbf{Z}_0} \int_{|\boldsymbol{\xi}|=1} |\mathbf{Z}_0^{-1}\boldsymbol{\xi}|^{-3} \widetilde{\mathbb{H}}(\boldsymbol{\xi})\, dS, \tag{26}$$

where $\widetilde{H}_{ijkl} = \widetilde{K}^{-1}_{ik} \xi_j \xi_l$ with $\widetilde{K}_{ik} = \widetilde{L}_{ijkl} \xi_j \xi_l$ and dS is an infinitesimal area element on the unit sphere characterized by $|\boldsymbol{\xi}| = 1$. Note that both $\widetilde{\mathbb{L}}$ and $\widetilde{\mathbb{P}}$ have major but not minor symmetries.

To summarize, the computation of the phase averages $\overline{\mathbf{F}}^{(r)}_l$ of the deformation gradient in the LCC that are essential for computing the effective potential $\widehat{W}$ for the polycrystal via (19), amounts to just solving the system of coupled nonlinear algebraic Eqs. (24) and (25), subject to (23), for the concentration tensors $\mathbb{A}^{(r)}$ and $\boldsymbol{a}^{(r)}$.

3.4. Evolution of microstructure

The above analysis makes use of a Lagrangian description of the kinematics. The evolution of the microstructure resulting from the finite changes in geometry are thus already accounted for in the homogenized stored-energy function $\widehat{W}$. This is in contrast to the corresponding results for viscoplastic polycrystals (see, e.g., Lebensohn et al., 2007), which are usually cast within an Eulerian description and do require additional computation of the evolution of the crystallographic and morphological texture. However, although not needed to determine the effective behavior, it is still of interest to have direct access to variables characterizing the microstructure evolution, as they provide deeper insight into the macroscopic response and possible development of instabilities.

In this work, we will focus on the study of the average deformation behavior of the grains through the evolution of certain average microstructural variables. Given the information that is available from the TSO homogenization method, it proves expedient – as a first approximation – to base the relevant variables on the average deformation gradient $\overline{\mathbf{F}}^{(r)}_l$ in the grains of the LCC, as determined by relation (22). It should be remarked, however, that a more sophisticated – but also more computationally demanding – approach leading to more accurate estimates for averages quantities in polycrystals has been recently proposed by Idiart and Ponte Castañeda (2007).

Thus, for the lamellar TPEs considered here, three microstructural variables serving to characterize the evolution of the deformations in each grain are identified (see Fig. 1 for a graphical illustration of these variables): (*i*) the average orientation of the layers within the grains, which evolves from $\mathbf{N}^{(r)}$ to $\mathbf{n}^{(r)}$, (*ii*) the average repeat length, which evolves from an initial value L_0 to a current value $L^{(r)}$, and (*iii*) the average shear angle along the layers, which starts from a zero initial value and evolves to a current value $\beta^{(r)}$. In terms of the phase averages $\overline{\mathbf{F}}^{(r)}_l$, the equations defining these variables read simply as (Lopez-Pamies and Ponte Castañeda, 2009)

$$\mathbf{n}^{(r)} = \frac{\overline{\mathbf{F}}^{(r)-T}_l \mathbf{N}^{(r)}}{|\overline{\mathbf{F}}^{(r)-T}_l \mathbf{N}^{(r)}|}, \quad L^{(r)} = |\overline{\mathbf{F}}^{(r)-T}_l \mathbf{N}^{(r)}|^{-1} L_0, \tag{27}$$

and

$$\beta^{(r)} = \cos^{-1}\left(\frac{\overline{\mathbf{F}}^{(r)}_l \mathbf{N}^{(r)}}{|\overline{\mathbf{F}}^{(r)}_l \mathbf{N}^{(r)}|} \cdot \mathbf{n}^{(r)}\right). \tag{28}$$

Here, the evolution of $\mathbf{n}^{(r)}$ physically describes the average rotation of the layers within the grains, which can act as a dominant geometric softening/stiffening mechanism of deformation. Note that, unlike the corresponding result of Read et al. (1999), the above result for (the evolution of) $\mathbf{n}^{(r)}$ is valid for arbitrarily large strains, as long as the solution remains on the principal path. Moreover, the variables $L^{(r)}$ and $\beta^{(r)}$ serve to measure, respectively, how much the hard and soft layers deform.

In view of the large number N of grain orientations, it proves useful to introduce a continuous ODF in the deformed configuration – analogous to the undeformed- configuration ODF (6) – serving to characterize the evolution of the distribution of the average orientations $\mathbf{n}^{(r)}$ as the deformation progresses. Thus, denoting by the unit vector $\mathbf{n}$ the continuum version of the discrete lamination directions $\mathbf{n}^{(r)}$, the current ODF p is defined via

$$c = \int_{\mathscr{S}} p(\mathbf{n}) dS, \quad \text{with} \quad \int_{\mathscr{F}} p(\mathbf{n}) dS = 1, \tag{29}$$

where c is the volume fraction of grains with current orientations in the solid angle $\mathscr{S} \subseteq \mathscr{F}$, with $\mathscr{F}$ denoting the unit hemisphere (or unit semicircle in two dimensions). The function p provides a convenient way to represent the evolution of the crystallographic texture by plotting p as a function of the current orientation $\mathbf{n}$ for increasing values of the deformation $\mathbf{F}$. Similarly, the continuum microstructural variables L and β can also be conveniently visualized as functions of the current orientation $\mathbf{n}$.

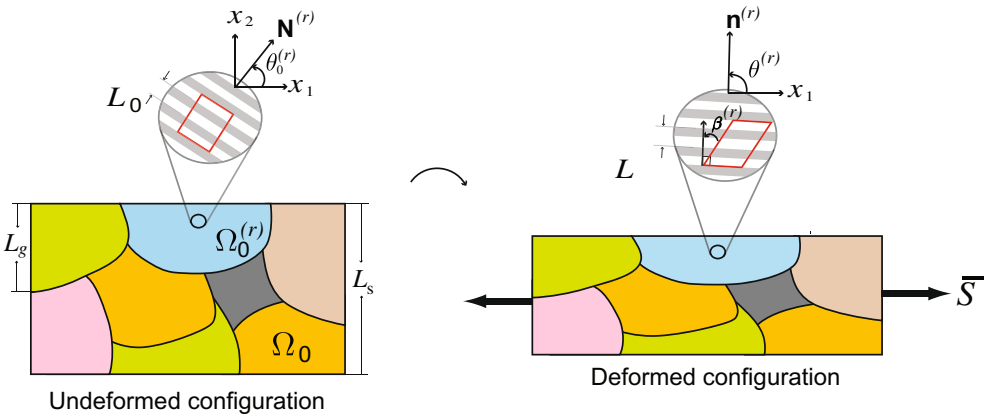

Fig. 1. Schematic of the two-scale microstructure of lamellar TPEs and microstructural variables. The characteristic length of the specimen L_s, the grain size L_g, and the repeat length L_0 are assumed to be well separated in the sense that $L_s \gg L_g \gg L_0$.

4. Results and discussion

In this section, the homogenization-based constitutive framework developed in Sections 2 and 3 is employed to investigate the macroscopic response and stability of a model class of lamellar TPEs with both "unoriented" and "oriented" crystallographic textures. The focus of this study will be on the elastic constitutive response, and on the possible development of elastically driven instabilities. As already mentioned, under certain types of loading conditions, plastic deformation can take place in the hard phase of lamellar TPEs and control the overall response beyond a certain elastic regime eventually leading to plastic instabilities (Cohen et al., 2000). Accordingly, a complete understanding of the mechanical behavior of TPEs under general loading conditions requires consideration of the plastic deformation of the hard (glassy or semi-crystalline) blocks. The effect of this plastic deformation is expected, however, to be largely dependent on the specific constitutive model (see, e.g. Lopez-Pamies et al., 2008) and is beyond the scope of this paper. Here, we will be satisfied to provide only a rough estimate for when the plastic deformation initiates and could start playing a significant role by monitoring the von Mises equivalent stress in the hard phase, as described further below. In summary, the main aims of this section are to examine in detail the following issues for lamellar TPEs:

- the key microscopic deformation mechanisms that lead to the onset of macroscopic elastic instabilities,
- the sensitivity of the macroscopic constitutive response and stability to the initial crystallographic texture,
- the sensitivity of the macroscopic constitutive response and stability to the heterogeneity contrast between the hard and soft phases, as well as to the compressibility of the soft phase.

Within the formulation proposed in this work, there are four specific inputs that are needed to determine the elastic response of lamellar TPEs under large strains: (*i*) the initial shape tensor $\mathbf{Z}_0$ that serves to characterize the initial shape of the grains, (*ii*) the initial ODF and the associated initial grain volume fractions $c_0^{(r)}$ that describe the initial distribution of lamination directions $\mathbf{N}^{(r)}$, (*iii*) the hyperelastic potentials that characterize the constitutive response of the hard and soft phases in the lamellar grains, and (*iv*) the macroscopic deformation gradient $\bar{\mathbf{F}}$ that describes the applied boundary conditions. The specific choices of each of these inputs are discussed in detail in the following paragraphs.

Initial shape tensor $\mathbf{Z}_0$. As discussed, for instance, in Honeker and Thomas (1996), standard processing methods for lamellar TPEs lead to sheets of these materials where the individual crystals tend to be cylindrical in shape with the long axis perpendicular to the plane of the sheet and with an average cross-section of elliptical shape (see Fig. 1). Therefore, the average grain shape in the undeformed configuration is taken here to be cylindrical, with elliptical symmetry in the plane transverse to the cylindrical axis. In this case, the microstructural tensor (26) takes the form

$$\widetilde{P}_{ijkl} = \frac{w_0}{2\pi} \int_{\xi_1^2+\xi_2^2=1} \frac{\widetilde{H}_{ijkl}(\xi_1,\xi_2,0)}{\xi_1^2 + w_0^2\xi_2^2}\, dS, \tag{30}$$

where the components are given with respect to the principal axes $\mathbf{e}_k$ of the shape tensor $\mathbf{Z}_0 = w_0\, \mathbf{e}_1 \otimes \mathbf{e}_1 + \mathbf{e}_2 \otimes \mathbf{e}_2$. Note that while the unit vector $\mathbf{e}_3$ is along the cylindrical axis, the vectors $\mathbf{e}_1, \mathbf{e}_2$ are along the minor and major axes of the elliptical symmetry in the transverse plane. When the grains are further assumed to be "equi-axed" in the transverse plane – as it will be done in the calculations shown below – the aspect ratio $w_0 = 1$.

Initial ODF. Experimental observations also suggest that the layers within the grains of typical lamellar TPEs tend to be aligned with the cylindrical axis of the grains (and perpendicular to the sheet). Because of this and for simplicity, the initial stacking directions of the lamellae are restricted here to lie in $x_1 - x_2$ plane such that

$$\mathbf{N}^{(r)} = \cos(\theta_0^{(r)})\mathbf{e}_1 + \sin(\theta_0^{(r)})\mathbf{e}_2 \quad (r = 1, \ldots, N), \tag{31}$$

where $\theta_0^{(r)}$ are the initial grain orientation angles (see Fig. 1). In the calculations below, detailed investigations will be

conducted for two kinds of initial distribution of stacking directions within the $x_1 - x_2$ plane: "unoriented" corresponding to an isotropic distribution in the plane (see Section 4.1), and "oriented" corresponding to a Gaussian distribution of orientations in the plane (see Section 4.2). In all the calculations, $(N =)40$ uniformly distributed initial grain orientation angles $\theta_0^{(r)}$ are used. Numerical experimentation shows that larger numbers of initial lamination directions ($N > 40$), or the way they are chosen (uniformly or randomly) has a marginal effect on the macroscopic stress-strain response and microstructure evolution, and only a small effect on the onset of macroscopic instabilities.

Constitutive behavior for the phases. For actual lamellar TPEs, fairly elaborate potentials (see, e.g., Lopez-Pamies et al., 2008) are necessary to accurately account for plastic deformations in the hard (glassy or semi-crystalline) phase and the strongly non-linear elastic deformations in the soft (rubbery) phase. However, since the primary aim of this paper is to investigate the generic effect of the elastic properties of the phases in the lamellar grains, and of the microstructure, on the overall behavior, microstructure evolution, and the onset of macroscopic elastic instabilities, simple compressible Neo-Hookean potentials allowing for thorough parametric analyses are chosen to describe the hard and soft phases. Thus, the potentials for the phases are taken to be of the form

$$W_c^{(p)}(\mathbf{F}) = \frac{\mu^{(p)}}{2}(\mathbf{F}\cdot\mathbf{F} - 3) - \mu^{(p)}\ln(\det\mathbf{F}) + \left(\frac{k^{(p)}}{2} - \frac{\mu^{(p)}}{3}\right)(\det\mathbf{F} - 1)^2 \quad (p = 1, 2), \tag{32}$$

where $\mu^{(p)}, k^{(p)}$ $(p = 1, 2)$ are the initial shear and bulk moduli of the soft and hard phases, respectively. For later reference, it is useful to define the heterogeneity contrast parameter $t = \mu^{(2)}/\mu^{(1)} \geqslant 1$ and the "Poisson's ratio" $\nu^{(p)} = (3k^{(p)} - 2\mu^{(p)})/(6k^{(p)} + 2\mu^{(p)})$. Throughout this section, the Poisson's ratio of the hard phase will be taken to be $\nu^{(2)} = 0.33$, while that of the soft phase $\nu^{(1)}$ will be allowed to vary in the range $\nu^{(1)} \in [0, 0.5]$, with the limiting value $\nu^{(1)} = 0.5$ corresponding to the case of incompressible behavior.

Even though the constitutive potentials (32) are purely elastic, they still allow to compute an estimate for when the onset of plastic deformation in the hard blocks of the lamellae may become important. Indeed, since the average deformation gradient in grains with orientation r are approximately given by $\overline{\mathbf{F}}_l^{(r)}$, the corresponding average deformation gradient in the hard phase $\mathbf{F}_h^{(r)}$ can be readily computed from Eqs. (14) and (15) with $\mathbf{F} = \overline{\mathbf{F}}_l^{(r)}$. Then, the average Piola-Kirchhoff and Cauchy stresses in the hard phase of orientation r may be computed, to a first approximation, via

$$\mathbf{S}_h^{(r)} = \frac{\partial W_c^{(2)}}{\partial \mathbf{F}}(\mathbf{F}_h^{(r)}), \quad \boldsymbol{\sigma}_h^{(r)} = \frac{1}{\det\mathbf{F}_h^{(r)}}\mathbf{S}_h^{(r)}\mathbf{F}_h^{(r)T}, \tag{33}$$

from which the von Mises equivalent stress in the hard phase of orientation r can in turn be computed via

$$\sigma_e^{h(r)} = \sqrt{\frac{3}{2}\boldsymbol{\sigma}_h^{\prime(r)}\cdot\boldsymbol{\sigma}_h^{\prime(r)}} \quad \text{with} \quad \boldsymbol{\sigma}_h^{\prime(r)} = \boldsymbol{\sigma}_h^{(r)} - \frac{1}{3}\sigma_{h\,kk}^{(r)}\mathbf{I}. \tag{34}$$

Thus, by comparing the von Mises equivalent stress $\sigma_e^{h(r)}$ with the value of the yield stress σ_y of the hard (glassy or semi-crystalline) phase, we may obtain a "crude" estimate for when the plastic effects start to play a role, and possibly modify the conclusions of our analyses based on purely elastic deformations. In this work, based on the normalized yield stress for polystyrene in SBS – the most widely used thermoplastic elastomer – plastic yielding in grains with a given orientation r is estimated to take place when

$$\sigma_e^{h(r)} \geqslant \sigma_y \approx 7\mu^{(1)} \tag{35}$$

We conclude this remark by re-emphasizing that the constitutive framework proposed here applies equally well to more sophisticated potentials (not just Neo-Hookean) including those that are commonly used in the context of finite-strain J_2 deformation theory of plasticity (Hutchinson and Neale, 1981), which would permit a more detailed study of the plastic deformation of the hard phase. Indeed, preliminary calculations show that the results for the "principal" solution and the associated macroscopic instabilities are not qualitatively affected by the constitutive model chosen for the hard phase.

Applied loading conditions. Motivated by the available experimental data (see, e.g., Honeker and Thomas, 1996; Garcia, 2006), we focus on macroscopic deformation gradients that are consistent with a uni-axial state of stress in the x_1-axis. Therefore,

$$\overline{\mathbf{F}} = \overline{F}_{ij}\,\mathbf{e}_i \otimes \mathbf{e}_j \quad (i, j = 1, 2, 3) \tag{36}$$

is chosen such that the macroscopic first Piola-Kirchhoff stress

$$\overline{\mathbf{S}} = \frac{\partial\widehat{W}}{\partial\mathbf{F}}(\overline{\mathbf{F}}) = \overline{S}\,\mathbf{e}_1 \otimes \mathbf{e}_1. \tag{37}$$

Within this context, for convenience, $\overline{F}_{11} = \overline{\lambda}$ is chosen as the loading parameter and the rest of the eight components of the deformation gradient are determined such that the corresponding eight components of the stress tensor are identically zero and the stress state is therefore uniaxial. From a computational point of view, it is important to recognize that for the material systems with the microstructure dictated by (30) and (31), Neo-Hookean hard and soft phases (32), and uni-axial loading conditions (37) of interest here, the problem to be solved becomes two-dimensional (generalized plane strain).

4.1. Unoriented samples

In this subsection we examine in detail the behavior of the model class of lamellar TPEs described above with *unoriented* crystallographic texture. Specifically, we consider samples with cylindrical grains with circular cross section and an isotropic distribution of stacking directions in the transverse $(x_1 - x_2)$ plane, for which the initial ODF is simply given by

$$p_0(\theta_0) = \frac{1}{\pi} \quad \text{with} \quad 0 \leqslant \theta_0 \leqslant \pi. \tag{38}$$

The initial grain angles and the associated grain volume fractions may then be taken as

$$\theta_0^{(r)} = \frac{r - 1/2}{N}\pi, \quad c_0^{(r)} = \frac{1}{N} \quad (r = 1, \ldots, N). \tag{39}$$

This subsection is organized as follows. The theoretical predictions for the macroscopic stress–stretch response and onset of macroscopic (long-wavelength) instabilities, as a function of elastic properties of the phases, are presented in Figs. 2 and 3. The deformation mechanisms responsible for the onset of macroscopic instabilities and the effect of elastic properties of the phases on the deformation mechanisms, are then investigated in Figs. 4–6. It must be remarked that macroscopic instabilities, whose onset is marked by the loss of strong ellipticity (LSE) of the homogenized specimen, typically manifest themselves in the form of localized bands of deformation. Though narrow as compared to the specimen dimensions, the bands are much wider than the average grain size. In addition, microscopic instabilities, e.g. of buckling type with wavelengths on the order of grain size or less, may occur earlier than the long wavelength instabilities but they cannot be

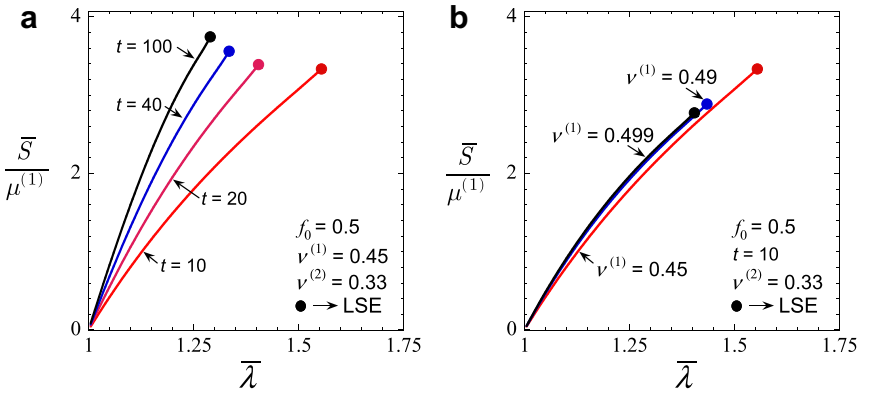

Fig. 2. Uniaxial stress–stretch curves for an unoriented specimen subjected to uniaxial tension. (a) Effect of contrast parameter t. (b) Effect of Poisson's ratio of the soft phase $\nu^{(1)}$. (Loss of strong ellipticity (LSE) is indicated by the full circles.)

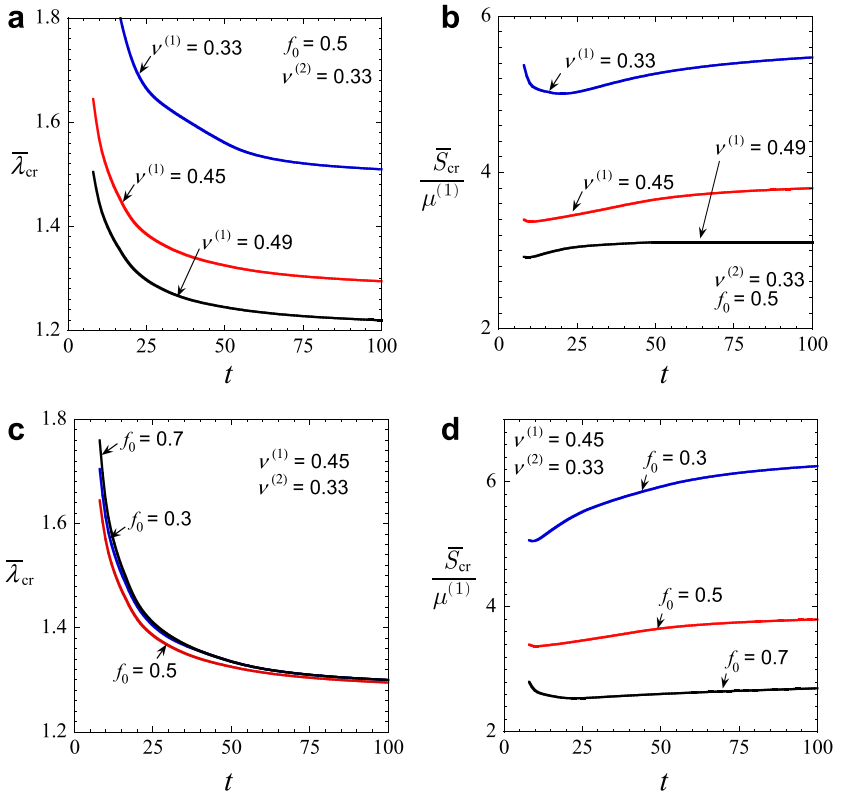

Fig. 3. Critical stretch and critical stress at LSE as a function of contrast parameter t in unoriented specimens subjected to uniaxial tension. (a and b) Effect of Poisson's ratio $\nu^{(1)}$. (c and d) Effect of initial volume fraction of the soft phase f_0.

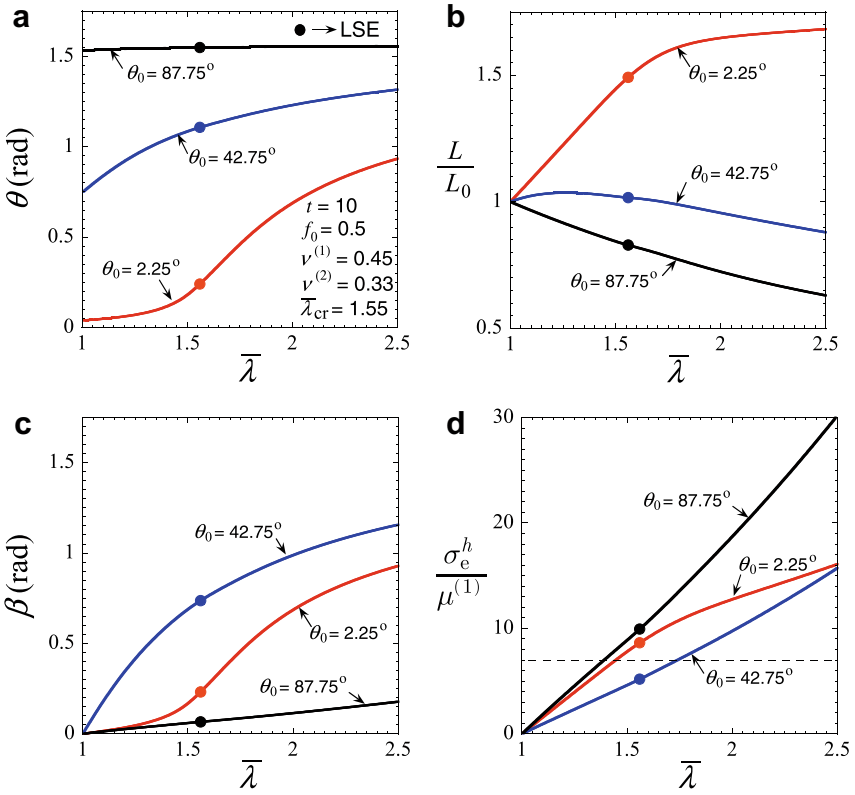

Fig. 4. Evolution of microstructural variables and average effective stress in the hard phase of the lamellae, for three different grains, in an unoriented specimen subjected to uniaxial tension for the soft phase initial volume fraction $f_0 = 0.5$, contrast in shear moduli of the phases $t = \mu^{(2)}/\mu^{(1)} = 10$, initial Poisson's ratio of the soft phase $\nu^{(1)} = 0.45$, and initial Poisson's ratio of the hard phase $\nu^{(2)} = 0.33$. (a) Average current lamination angle θ in three grains composed of lamellae that are nearly perpendicular ($\theta_0 = 2.25^\circ$), diagonal ($\theta_0 = 42.75^\circ$) and parallel ($\theta_0 = 87.75^\circ$) to the stressing direction x_1 in the undeformed configuration. (b) Average repeat length ratio L/L_0. (c) Average shear angle β. (d) Average effective stress in the hard phase of the lamellae σ_e^h normalized with respect to the initial shear modulus of the soft phase $\mu^{(1)}$. The dashed line represents yielding for the hard phase based on the yield stress for polystyrene in SBS.

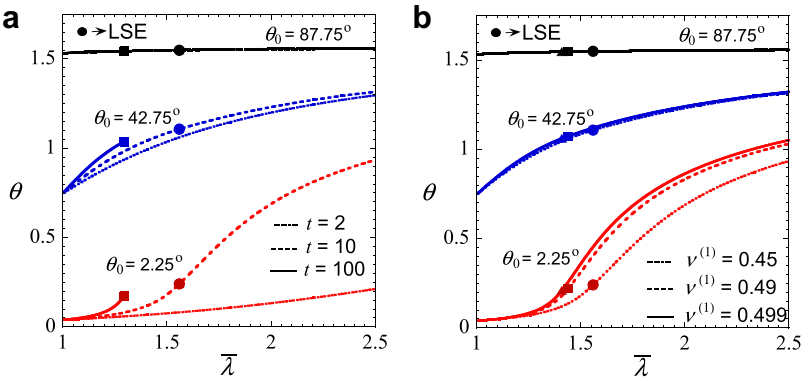

Fig. 5. Evolution of current lamination angle in an unoriented sample subjected to uniaxial tension for three grains that are initially (nearly) perpendicular ($\theta_0 = 2.25^\circ$), diagonal ($\theta_0 = 42.75^\circ$) and parallel ($\theta_0 = 87.75^\circ$) to the stressing direction x_1. (a) Effect of contrast parameter t for $f_0 = 0.5$, $\nu^{(1)} = 0.45$, and $\nu^{(2)} = 0.33$. (b) Effect of Poisson's ratio of the soft phase $\nu^{(1)}$ for $t = 10$, $f_0 = 0.5$, and $\nu^{(2)} = 0.33$.

captured using the framework adopted here. Nevertheless, LSE provides an upper limit for the onset of these instabilities (Geymonat et al., 1993).

Fig. 2 shows the macroscopic stress–stretch response of unoriented specimens, subjected to uniaxial tension, as a function of elastic properties of the phases. It is plain that the macroscopic stiffness increases with increasing contrast but is fairly insensitive to the Poisson's ratio of the soft phase, particularly close to the incompressibility limit. Furthermore, the stiffness is a non-trivial function of the

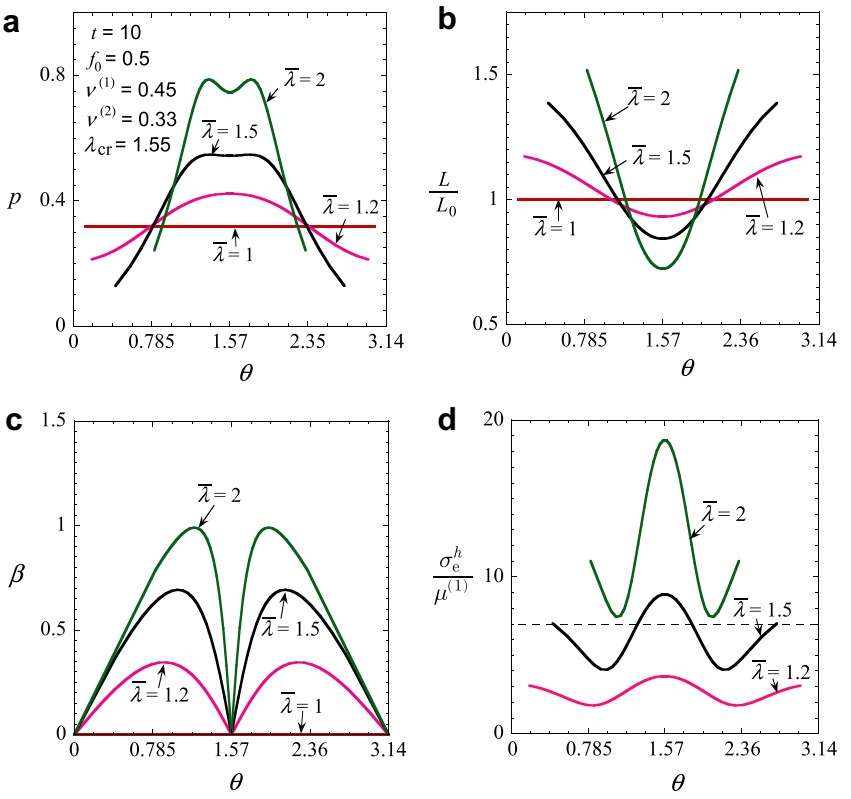

Fig. 6. Evolution of (a) orientation distribution function p, (b) average repeat length ratio L/L_0, (c) average shear angle β, and (d) Average effective stress in the hard phase of the lamellae σ_e^h normalized with respect to the initial shear modulus of the soft phase $\mu^{(1)}$ in grains in an unoriented specimen subjected to uniaxial tension. The dashed line represents yield surface for the glassy phase based on the normalized yield stress for polystyrene in SBS.

elastic properties of the phases and the evolution of the microstructure – and not just a simple rule of mixtures. Remarkably, the model predicts LSE at a finite stretch $\bar{\lambda}_{cr}$, and no results are shown beyond this point. Furthermore, for all unoriented specimens subjected to uniaxial tension along the x_1 axis, at LSE, unit vectors $\mathbf{V} = \mathbf{e}_2$ and $\mathbf{u} = \mathbf{e}_1$ are found to minimize the product in Eq. (11), i.e. the localized band at LSE is found to be aligned with the tensile x_1-direction or perpendicular to the compressive x_2-direction (compression is induced by the Poisson effect). Thus, unoriented specimens typically lose strong ellipticity at $\bar{\lambda}_{cr}$, when the incremental modulus $\hat{L}_{1212}$ (shear modulus along the loading direction) vanishes. In this context it must be emphasized (see, e.g., Vogler et al., 2001) that experimental observations of instabilities are usually *post mortem* and therefore correspond to the final configuration of the specimen, which necessarily involve the post-bifurcation solution and may look quite different from the above-described initial instability mode, which is based on the "principal" solution. Nevertheless, the critical deformation predicted by this approach should still provide a reasonable estimate for the possible onset of the experimentally observed instabilities.

Fig. 3 shows the critical stretch $\bar{\lambda}_{cr}$ and the corresponding critical stress $\bar{S}_{cr}$ at which LSE ensues, as a function of the contrast t, and Poisson's ratio and initial volume fraction of the soft phase, $\nu^{(1)}$ and f_0, respectively. Note that no instabilities are predicted by the analysis at small contrasts (t less than about 5), and that, in general, the larger the contrast the smaller the stretch and stress at which loss of strong ellipticity ensues. In general, the critical stretch seems to be more sensitive to the contrast than the critical stress, while the critical stress is more sensitive to the volume fraction of the hard and soft phases than the critical stretch. On the other hand, both the critical stress and stretch are equally sensitive to the Poisson's ratio of the soft phase.

As mentioned earlier, the proposed theory may also be used to investigate deformation mechanisms, leading to LSE, by analyzing the evolution of the microstructural variables introduced in Section 3.4. In addition, the Von Mises equivalent stress in the hard phase of the lamellar grains may be used to estimate as to when the plastic effects may start to become important. In this regard, we depict in Fig. 4 the evolution of the microstructural variables θ, L, β and the von Mises equivalent stress in the hard phase σ_e^h in an unoriented specimen subjected to uniaxial stress along the x_1 axis. We focus our attention on three particular initial grain orientations: perpendicularly oriented ($\theta_0 = 2.25^\circ$), diagonally oriented ($\theta_0 = 42.75^\circ$), and parallelly oriented ($\theta_0 = 87.75^\circ$). The results shown are for contrast $t = \mu^{(2)}/\mu^{(1)} = 10$, Poisson's ratio of the soft phase $\nu^{(1)} = 0.45$, and initial volume fraction of the soft phase $f_0 = 0.5$. As expected, the deformation of the grains is

highly dependent on the initial grain orientation. Parallelly oriented grains ($\theta_0 = 87.75^\circ$) deform mainly through stretching of lamella, resulting in a monotonic increase in the equivalent stress in the hard phase and a steady decrease in repeat length ratio, while diagonally oriented grains ($\theta_0 = 42.75^\circ$) deform mainly via a combination of rigid rotation and shear along the lamella. In contrast, the perpendicularly oriented grains ($\theta_0 = 2.25^o$) deform differently at small and large stretches. At small overall stretches, these grains deform predominantly by stretching along the stacking direction, resulting in a steady increase in the repeat length ratio and an increase in the equivalent stress in the hard phase. However, this is an energetically unfavorable mode of deformation as an increasingly larger amount of energy is required to deform the hard phase, and a new deformation mode ensues, consisting of a combination of rigid rotation and shear along lamella, which results in a much slower increase in repeat length ratio and equivalent stress in the hard phase of the lamellae. This transition from a "high-energy" to a "lower-energy" deformation mode is responsible for the drop in the shear stiffness (i.e., in L_{1212}) of the material along the tensile direction, which results in LSE. Here, it is important to remark that the results shown beyond the LSE correspond to the "principal" solution, and are shown only to highlight the trends in the principal solution, but are not meant to be interpreted as the actual solution beyond LSE.

To better understand the effect of the elastic properties of the phases on the onset of the macroscopic instabilities, Fig. 5 shows results for the evolution of grain orientations – for the same set of grains as in Fig. 4 (i.e. for $\theta_0 = 2.25$, 42.75, and 87.75°) – for different values of the contrast and Poisson's ratio of the soft phase. It can be seen from the figure that evolution of grain orientation θ, particularly for perpendicularly oriented grains, is strongly dependent on the elastic properties of the phases. More specifically, the larger the contrast t or the larger the Poisson's ratio of the soft phase $\nu^{(1)}$, the earlier and sharper the transition in deformation mode. This correlates well with the corresponding plots in Fig. 3 that also show earlier instabilities (LSE) for larger contrast or larger Poisson's ratio. Interestingly, there is very little effect of t and $\nu^{(1)}$ on the evolution of initially parallelly and diagonally oriented grains. This fact, which is plausible from a physical view point, seems to corroborate the hypothesis that the development of the elastic macroscopic instabilities is directly linked to the change in deformation mode of the perpendicularly oriented grains.

A more complete picture of the evolution of the microstructural variables is provided in Fig. 6, which shows plots for the ODF p, microstructural variables L and β, and von Mises equivalent stress in the hard phase σ_e^h, as a function of the current grain orientation θ. Fig. 6a shows the ODFs, indicating the probability p of finding grains with a certain grain angle θ in the deformed configuration, for three different stretches for the same set of material parameters and loading conditions as in Fig. 4. The ODFs evolve quite rapidly, particularly for deformations near LSE ($\bar{\lambda}_{cr} = 1.55$). At and beyond LSE, the majority of the lamellae exhibit approximately a ±20° misalignment with the stressing direction resulting in a "double-bump" pattern in the ODF. This remarkable result is consistent with the recent experimental observations of Garcia (2006) (see Fig. V.16), which also show the transition from a single-mode to a bimodal distribution of orientations. As seen from Fig. 4b–d, this transition is clearly due to the fact that while lamellae aligned with the stretching direction deform by stretching the hard phase (there is no alternative for these orientations), "unfavorably" oriented lamellae deform mainly via shearing of the soft phase, which is energetically preferable. It is relevant to remark that these observations are also in very good qualitative agreement with uniaxial tension experiments on isotropic lamellar TPEs (Séguéla and Prud'homme, 1981) where at relatively small stretches, the initially randomly oriented lamella rotate such that majority of them align at around ±20 degrees from the stressing direction, resulting in the characteristic four-point small angle X-ray scattering (SAXS) patterns.

In addition, it is noted that the dashed lines in Figs. 4d and 6d correspond to the above-mentioned estimate (35) for plastic yield in the hard phase. They show that, as would be expected, parallelly oriented grains are the first to undergo plastic yielding followed by the perpendicularly oriented grains. Plastic yielding occurs in these grains just before the LSE. However, since the volume fraction of grains that undergo plastic yielding before the onset of macroscopic instabilities is relatively small, the estimates for microstructure evolution and macroscopic response presented above are expected to be reasonably accurate until the LSE.

Finally, in Fig. 7, comparisons are presented with the FEM results of Tzianetopoulou (2007) for plane strain extension of several realizations of polygranular systems with random orientations and hexagonal grains. (In this plot and for this plot only, we have changed the uniaxial loading condition described by expression (37) to match the plane strain extension conditions used in the numerical simulations). More specifically, our model predictions for the average Cauchy stress versus the average stretch are compared in this figure with the FEM results for 3

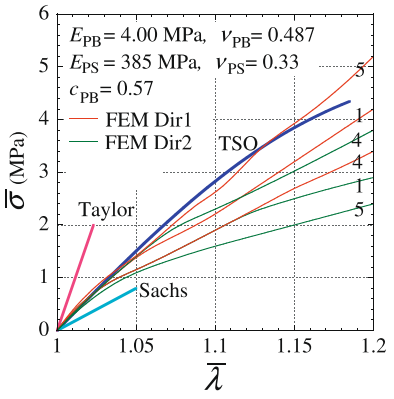

Fig. 7. Comparison of homogenization estimates (TSO) with FEM simulations of Tzianetopoulou (2007) and Taylor- and Sachs-type estimates for plane strain extension: macroscopic Cauchy stress versus macroscopic stretch. FEM results labeled 1, 4 and 5 are for 3 different realizations subjected to plane strain tension along two perpendicular directions (directions 1 and 2).

different realizations (RVEs 1, 4, and 5) subjected to plane strain tension along two perpendicular directions (directions 1 and 2). As can be seen from the figure, the results for each realization are not quite isotropic, and they differ from one realization to the other. This is, of course, to be expected given the statistical nature of the problem. Detailed comparisons with our model predictions, which are essentially isotropic by construction, would require a larger set of realizations and ensemble averages to be performed. However, it can be seen from the figure that, although a little bit stiffer than the rough average of the given FEM realizations, the model predictions are consistent with these results. Certainly, they exhibit very good agreement for small strain, when the effect of differences in the various realizations are expected to be relatively small, and consistent with the FEM results, they are much softer than the Taylor-type estimate, and also quite a bit stiffer than the Sachs-type estimate. Also, it should be pointed out that as already discussed in the context of our model predictions, the FEM simulations of Tzianetopoulou (2007) also exhibit the development of extra peaks in the ODFs with increasing deformation. However, detailed comparisons were not possible due to apparent differences in the definitions used for the ODFs in this work. Of course, the FEM simulations also include valuable information about the local distributions of the fields in the polycrystals, and the reader is referred to Tzianetopoulou (2007) for more details on this.

4.2. Oriented samples

Next, we examine the behavior of lamellar TPEs with *oriented* crystallographic texture. In this case, the initial distribution of lamination directions is characterized by a Gaussian-like ODF of the form (see Fig. 11)

$$p_0 = \frac{1}{z_0} e^{-\frac{\mathbf{N}'\cdot\mathbf{N}'}{2\ \sigma^2}}, \quad \mathbf{N}' = \mathbf{N} - \boldsymbol{\mu}, \tag{40}$$

where $\boldsymbol{\mu} = \cos(\theta_0^m)\ \mathbf{e}_1 + \sin(\theta_0^m)\ \mathbf{e}_2$ denotes the (bias) mean stacking direction, θ_0^m denotes the angle between the stressing direction and the mean stacking direction, σ characterizes the width of initial distribution of stacking directions, $\mathbf{N} = \cos(\theta_0)\ \mathbf{e}_1 + \sin(\theta_0)\ \mathbf{e}_2$ with $(\theta_0^m - \pi/2) \leqslant \theta_0 \leqslant (\theta_0^m + \pi/2)$, and the constant

$$z_0 = \int_{\theta_0^m-\pi/2}^{\theta_0^m+\pi/2} e^{-\frac{\mathbf{N}'\cdot\mathbf{N}'}{2\ \sigma^2}} d\theta_0, \quad \text{with} \quad \int_{\theta_0^m-\pi/2}^{\theta_0^m+\pi/2} p_0 d\theta_0 = 1. \tag{41}$$

The initial grain angles and the associated grain volume fractions are then taken to be

$$\begin{aligned} \theta_0^{(r)} &= \theta_0^m - \theta_0^s + (r - 1/2)\ \delta\theta_0 \quad \text{and} \\ c_0^{(r)} &= \int_{\theta_0^m-\theta_0^s+(r-1)\delta\theta_0}^{\theta_0^m-\theta_0^s+r\delta\theta_0} p_0(\theta_0) d\theta_0, \end{aligned} \tag{42}$$

where $\theta_0^s = 4\sigma$ and $\delta\theta_0 = 8\sigma/N$ for $\sigma^2 << 1$ and $\theta_0^s = -\pi/2$ and $\delta\theta_0 = \pi/N$ otherwise. Note that while $\theta_0^m = 0^\circ$ corresponds to the limiting case when the stressing direction is perpendicular to the lamella, $\theta_0^m = 90^\circ$ corresponds to the case when the lamella are aligned with the stressing direction. Also note that $\sigma \to 0$ corresponds to the extreme case of a perfect laminate. In the other extreme case when $\sigma \to \infty$, (40) reduces to the unoriented distribution (38) studied in the preceding subsection.

Fig. 8 shows results for the Young's Modulus $E = d\bar{S}/d\bar{\lambda}(\bar{\lambda} = 1)$, as a function of the distribution parameter σ and loading angle θ_0^m. From the figure, it is evident that E is extremely sensitive to the initial distribution of stacking directions when evaluated along the lamella, i.e., for $\theta_0^m = 90^\circ$. By contrast, there is relatively little effect of the initial distribution of lamination directions on the Young's modulus along other loading directions ($\theta_0^m \leqslant 75^\circ$), even for reasonably broad initial distributions ($0.05 \leqslant \sigma \leqslant 0.1$). These observations indicate that assuming an oriented specimen to be a perfect laminate, while attempting to infer the elastic properties of the underlying soft and hard blocks from measurements of the macroscopic Young's moduli at different loading angles (as attempted, for instance, by Allan et al., 1991), can lead to erroneous results – namely, a considerable underestimation of properties of the hard phase, particularly its shear modulus – especially when the initial distribution of orientations is not narrow.

Fig. 9 shows plots of the macroscopic stress versus the macroscopic stretch in oriented specimens, subjected to uniaxial tension along the mean stacking direction, with initial distribution of stacking directions characterized by $\sigma = 0.1$ (see Fig. 11b). For comparison purposes, results are also included in dashed lines for a perfect crystal ($\sigma = 0$) with layer normal aligned with the tensile direction. Note that softening of the overall tensile response is observed only for imperfect samples with $\sigma = 0.1$. The softening in imperfect samples is attributed to the evolution of microstructure in this specimen, as will seen in more detail further below. Once again, loss of ellipticity is observed at a critical stretch $\bar{\lambda}_{cr}$, beyond which no results are shown. The model predicts that $\bar{\lambda}_{cr}$ depends strongly on the contrast t, and a little less strongly on the Poisson's ratio of the soft phase $\nu^{(1)}$. The results show that as was the case for the unoriented samples, the material loses ellipticity because the shear modulus L_{1212} (the shear modulus perpendicular the compressive direction) vanishes at $\bar{\lambda}_{cr}$.

Fig. 10 shows the critical stretch and corresponding critical stress at which macroscopic instabilities take place in oriented systems, under tensile loading perpendicular to the average layer direction, as a function of the elastic properties of the phases and initial distribution of stacking directions. Note from Fig. 10a and b that increasing the contrast t and increasing the Poisson's ratio of the soft phase $\nu^{(1)}$ leads to smaller critical stretches and stresses. Fig. 10c and d show that the initial width σ of the distribution of stacking directions has a moderate effect on both the critical stretch and stress for strongly aligned systems with $\sigma < 0.1$. However, the effect is more significant as σ increases beyond this level and results in a sizable delay in the possible onset of instabilities, which is consistent with the unoriented systems considered earlier (which correspond to the limit as $\sigma \to \infty$). Note also that higher contrasts leads to smaller (larger) critical stresses for $\sigma < 1 (\sigma > 1)$, while higher contrasts leads to smaller critical stretches that are independent of the value of σ.

Fig. 11 shows results for the evolution of grain orientation θ and von Mises equivalent stress σ_e^h in the hard phase

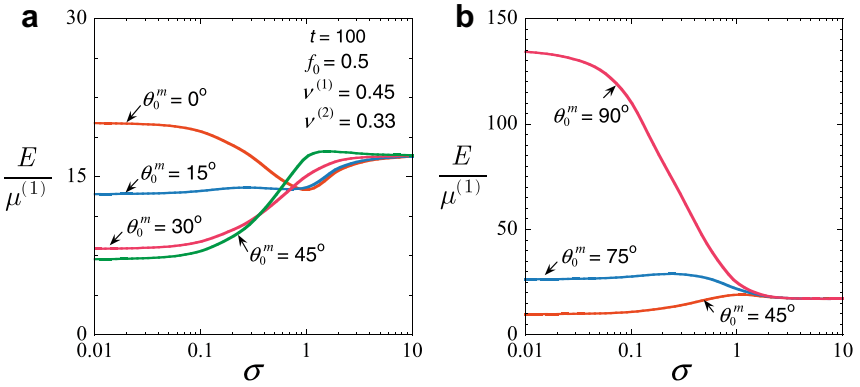

Fig. 8. Young's modulus of oriented specimen as a function of the variance σ of the initial orientation distribution for several angles θ_0^m between mean lamination direction and the stressing direction.

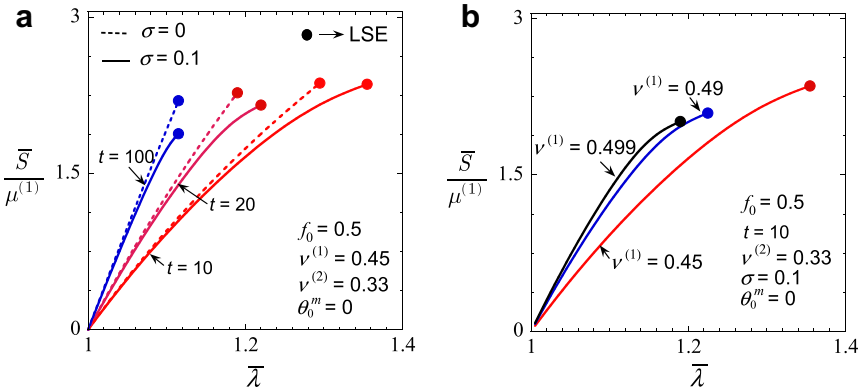

Fig. 9. Uniaxial stress–stretch curves for oriented specimens subjected to uniaxial tension along the mean stacking direction. (a) Effect of contrast in shear moduli of the phases t. (b) Effect of Poisson's ratio of the soft phase $\nu^{(1)}$.

of the lamellae – in a perpendicularly oriented grain ($\theta_0 \approx 2^\circ$) – for oriented specimens subjected to uniaxial tension along the mean stacking direction, for three different initial distributions of stacking directions with $\sigma = 0.04$, 0.1, and 0.2. Clearly, the deformation behavior of the perpendicularly oriented grains in oriented specimens is similar to that of the unoriented specimens. That is, while these grains deform mainly by stretching perpendicular to the lamellae at small stretches, they deform predominantly via a combination of rigid rotation and shear along the lamellae close to and beyond LSE. Therefore we can conclude that the transition from one deformation mode to a different one is once again the source for the predicted elastic instabilities. Furthermore, the narrower the initial distribution of stacking directions the sharper and earlier the transition in deformation mode for the perpendicularly oriented grains. Similar observations revealing such deformation mechanisms were also made by Lopez-Pamies et al. (2008) in the simpler setting of a nearly oriented specimen composed of only *two* slightly misoriented stacks of lamellae. Note from Fig. 11b that, at least until LSE, the von Mises equivalent stress in the hard of lamellae in perpendicularly oriented grains is much below the yield stress for the hard phase. Thus, the elastic instabilities are predicted to precede plastic instabilities in perpendicularly loaded oriented specimen, in agreement with experimental observations for this type of loading (Garcia, 2006).

For completeness, Fig. 12 shows evolution plots of the ODF as the deformation $\bar{\lambda}$ progresses all the way up to LSE at $\bar{\lambda}_{cr}$. Results are shown for two different values of the initial width σ (0.04 and 0,1) of the orientation distribution. It can be seen from these figures that the behavior is qualitatively similar for the two values of σ, consisting in the broadening and flattening of the peak, eventually leading to the development of a bimodal distribution about the symmetry direction ($\theta = 0^\circ$). The development of the double-bump in the distribution is again seen to be closely related to the above-mentioned sudden rotation of the perpendicularly oriented grains (with small values of θ_0) near the LSE point. Comparing with the corresponding results shown in Fig. 6a for the unoriented samples, it is interesting to remark that although the starting point is quite different – a flat distribution for the unoriented systems versus a highly peaked distribution for the oriented systems – the elastic instability is driven by the same physical mechanism of shear-and-rotation of the "unfavorably" oriented layers (i.e., those perpendicular to the tensile direction), leading to a transition from a unimodal distribution to a bimodal one.

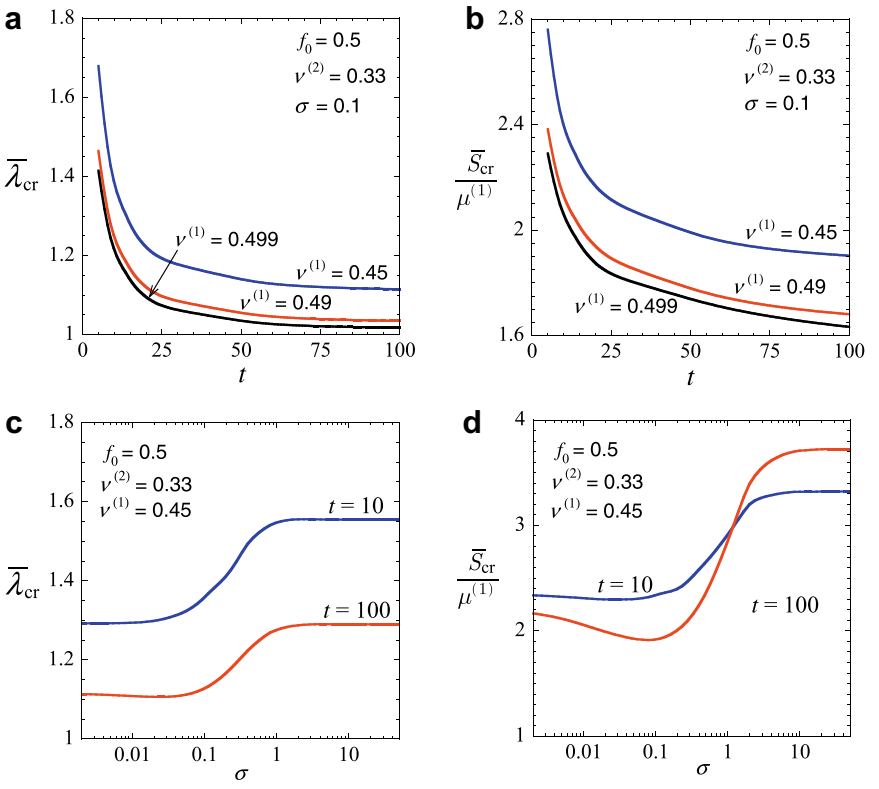

Fig. 10. Effect of contrast in shear moduli of the phases, distribution of initial lamination directions, and Poisson's ratio of the soft phase on critical stretch and critical stress at loss of strong ellipticity in perpendicularly loaded oriented specimens.

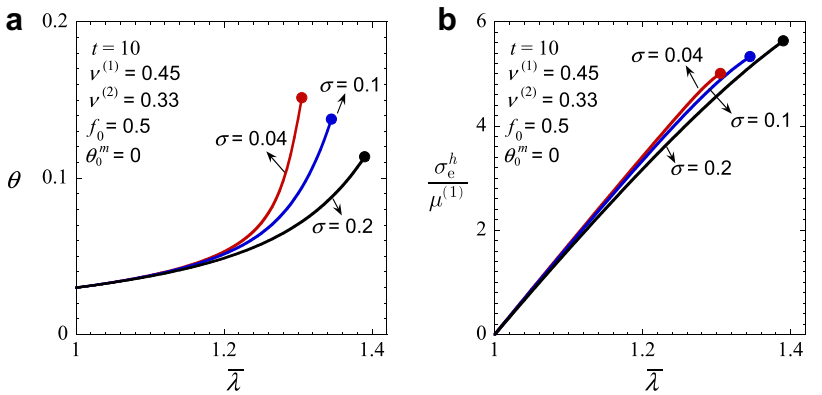

Fig. 11. Deformation behavior of a perpendicularly oriented grain in oriented specimens subjected to uniaxial tension along the mean stacking direction. (a) Evolution of grain orientation. (b) Evolution of von Mises equivalent stress in the hard phase of the lamellae.

Fig. 13 shows a comparison of the evolution of the ODF and macroscopic stress-strain response for uniaxial compression (C) with the prior results for tension (T) in an oriented sample. Fig. 13a again shows that the "unfavorably" oriented lamellae tend to rotate towards the stressing direction for uniaxial *tension* ($\bar{\lambda} > 1$), leading to the formation of a double-bump pattern. On the contrary, for uniaxial *compression* ($\bar{\lambda} < 1$), there are essentially no "unfavorably" oriented lamellae since most grains are aligned with the tensile direction that is induced by the Poisson effect in the direction perpendicular to the tensile direction. In fact, the layers still tend to rotate to align themselves with the tensile direction, but only slightly, and in this case it only leads to an increasingly sharper peak (in the ODF) at $\theta = 0^\circ$ as the deformation progresses. By comparing the macroscopic responses for tension and compression in Fig. 13b, it becomes even clearer that the stress-strain softening and LSE observed for uniaxial tension are the result of the comparatively large rotation and shear of the "unfavorably" oriented grains and *not* of the nonlinear

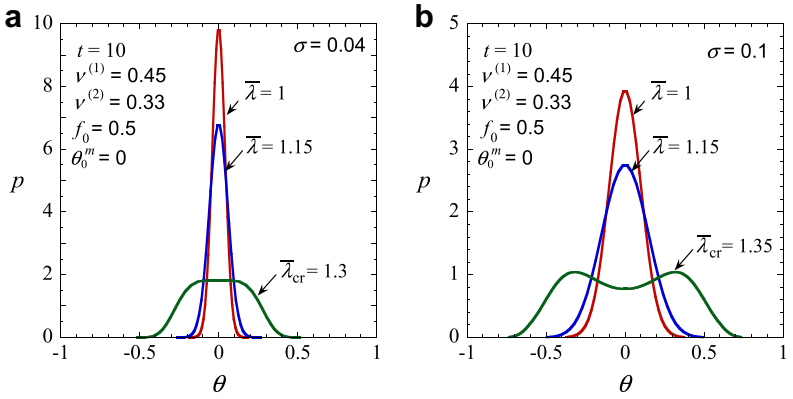

Fig. 12. Evolution of the ODF in oriented specimens subjected to uniaxial tension along the mean stacking direction for two different initial distributions of orientations.

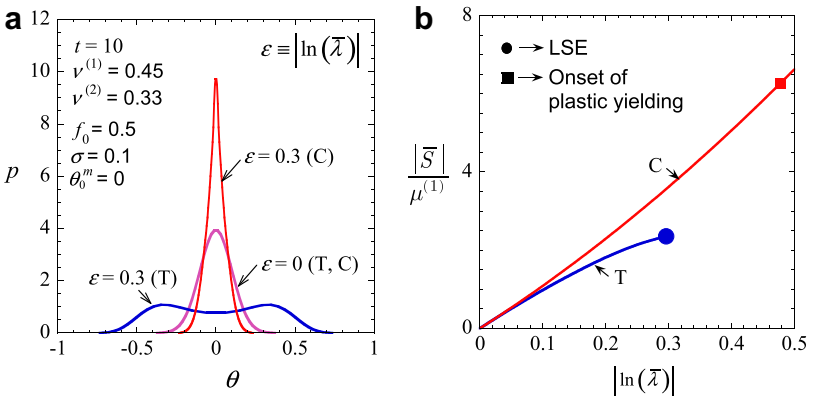

Fig. 13. Results for a perpendicularly loaded oriented specimen in tension (T) and compression (C). (a) Evolution of the ODF. (b) Uniaxial stress–stretch curves.

constitutive behaviors of the phases. On the other hand, for uniaxial compression, most layers are subjected locally to tension along their long dimension, which leads to plastic yielding and eventual failure of the layers. The critical strain for plastic yielding of layers, which happens almost simultaneously in nearly all the grains, is indicated by a full square in Fig. 13b.

5. Conclusions

A homogenization-based framework has been proposed to model hyperelastic polycrystals. The analytical framework allows for the efficient computation of variational estimates for the evolution of the microstructure and the macroscopic constitutive response of lamellar TPEs making direct use of the properties of the constituent blocks, initial distribution of lamination directions, average grain shape, and initial volume fractions of the blocks. Motivated by experimental observations for oriented sheet specimens prepared using the roll casting process (Honeker and Thomas, 1996) – and for simplicity – the average grain shape in the undeformed configuration was assumed here to be cylindrical with circular cross-section in the transverse $x_1 - x_2$ plane (the plane of the sheet). Furthermore, the initial lamination directions were restricted to lie in the $x_1 - x_2$ plane so that for loadings within the plane, the problem becomes two-dimensional (generalized plane strain). Two kinds of initial distributions of stacking directions were considered: *unoriented* corresponding to an isotropic distribution of lamination directions in the plane and *oriented* corresponding to a Gaussian distribution of lamination directions. In line with experiments on TPEs reported in the literature, the analysis is restricted to uniaxial loading in the $x_1 - x_2$ plane, the focus being the study of the generic effect of the elastic properties of the phases and of the initial microstructure on the macroscopic response of lamellar TPEs up to the possible onset of macroscopic elastic instabilities.

In unoriented samples, grains with lamellae that are nearly perpendicular, diagonal, and parallel to the stressing direction (in the undeformed configuration) exhibit contrasting behaviors. While the initially parallel and diagonal grains respectively deform by stretching along the lamellae and a combination of rigid rotation and shear along the lamellae, the initially perpendicular grains deform

predominantly by stretching along the stacking direction at small strains and via a combination of rigid rotation and shear along the lamellae soon after. The transition from the hard deformation mode (controlled by stretching of the hard phase) to the soft mode (controlled by shear of the soft phase and rotation of the layers) in the "unfavorably" oriented grains (i.e., those that are initially perpendicular to the tensile direction) leads to the onset of a macroscopic elastic instability. Furthermore, the lamellae in the grains tend to develop preferential orientations of about 20 degrees, symmetrically about the loading axis, leading to a transition from a "unimodal" to a "bimodal" distribution of orientations. (Similar observations have been made recently in the Ph.D. thesis of Tzianetopoulou (2007), who carried out detailed FEM simulations for the macroscopic response of polygranular specimens using various realizations of unoriented specimens subjected to plane strain conditions.) This reorganization of the orientation distribution of the grains leads to a shear-band instability at the macroscopic level that can be related microscopically to the formation of zig-zag chevron patterns in isotropic styrene-butadiene-styrene (SBS) block copolymers (Séguéla and Prud'homme, 1981; Garcia, 2006). This deformation mechanism and the associated macroscopic elastic instabilities were found to be strongly dependent on the heterogeneity contrast of the hard and soft blocks, as well as on the Poisson's ratio of the soft blocks, but weakly dependent on the volume fraction of the blocks. In addition, the critical stress at the onset of the macroscopic instabilities is found to be weakly dependent of the properties of the hard phase, particularly for large elastic contrasts. The situation is similar to that of fiber-reinforced elastomers, subjected to compression along the fibers, where for extremely stiff fibers the critical stress depends only on the properties of the elastomeric matrix and initial volume fraction of fibers (Agoras et al., 2009; Lopez-Pamies and Idiart, 2009). Furthermore, nearly all the grains behave elastically until the onset of macroscopic (elastic) instabilities indicating that plastic yielding of the hard (glassy or semi-crystalline) phase is expected to have a significant effect on the overall response only after the onset of the macroscopic instabilities.

In oriented specimens, the Young's modulus was found to be quite sensitive to the initial distribution of orientations, especially for loadings that are aligned with the mean layer direction: the broader the initial distribution, the greater the deviation of the Young's modulus (along the mean layer direction) relative to the corresponding perfect laminate. This could provide a possible explanation for the large scatter in experimentally measured (Allan et al., 1991; Cohen et al., 2000) Young's modulus along the lamellae in oriented SBS specimens. In oriented specimens subjected to uniaxial tension along the mean lamination direction $\overline{\mathbf{N}}$, herein referred to as "perpendicularly loaded" specimens, the microstructure evolution in the grains and their sensitivity to the elastic properties and initial volume fractions of the phases is similar to that in unoriented specimens. However, the transition in the deformation mode for the "unfavorably" oriented grains, leading to the development of macroscopic instabilities, is strongly dependent on the variance of the orientation distribution function, occurring much earlier and being more sensitive to the elastic properties of the phases for (perpendicular loading of) the oriented specimens than for the unoriented specimens. On the other hand, for parallel loading of the oriented specimens the proportion of unfavorably oriented grains is minimal and the evolution of the microstructure is quite different tending to increase (instead of decrease) the overall stiffness of the material, so that no elastic instabilities were detected. Instead the layers are expected to yield plastically and eventually break up at sufficiently large strains leading to a different type of instability which cannot be appropriately modeled with the present theory.

Although no direct comparisons with experiments have been attempted in this work, the encouraging predictions of the theoretical model for somewhat idealized constituent properties and microstructures suggest that the theory does contain many of the basic ingredients necessary to be able to handle more realistic (3D) microstructures and constitutive models for the constituents blocks of TPEs with lamellar microstructures. In addition, the general theory can be applied – with suitable extensions – for TPE with other domain structures, such as the cylindrical and spherical geometries (Honeker and Thomas, 1996), as well as to other polymeric systems with similar two-scale structure, such as certain types of semi-crystalline polymers, where similar chevron-type instabilities have also been observed (Krumova et al., 2006).

Acknowledgements

The work of V.R. and O.L.P. was supported by the Agence Nationale de la Recherche (France) and that of P.P.C. by the National Science Foundation (USA) through Grant CMMI–0654063. The authors would like to thank an anonymous reviewer for pointing us to the Ph.D. thesis of T. Tzianetopoulou. Some comparisons to this work were included in Fig. 7 at the suggestion of this reviewer.

References

Adams, B.L., Olson, T., 1998. The mesostructure-properties linkage in polycrystals. Progress in Material Science 43 (1), 1–87.

Agoras, M., Lopez-Pamies, O., Ponte Castañeda, P., 2009. Onset of macroscopic instabilities in fiber-reinforced elastomers at finite strain. Journal of the Mechanics and Physics of Solids 57, 1828–1850.

Allan, P., Arridge, R.G.C., Ehtaiatkar, F., Folkes, M.J., 1991. The mechanical properties of an oriented lamella stock formed from an SBS block copolymer. Journal of Physics D 24, 1381–1390.

Cheng, J.Y., Ross, C.A., Edwin, L.T., Vanessa, Z.H.C., Julius Vancso, G., Rob, G.H.L., 2001. Formation of a Cobalt magnetic dot array via block copolymer lithography. Advanced Materials 13 (15), 1174–1178.

Cohen, Y., Albalak, R.J., Dair, B.J., Capel, M.S., Thomas, E.L., 2000. Deformation of oriented lamellar block copolymer films. Macromolecules 33, 6502–6516.

deBotton, G., Ponte Castañeda, P., 1992. On the ductility of laminated materials. International Journal of Solids and Structures 29, 2329–2353.

Fredrickson, G.H., Bates, F.S., 1996. Dynamics of block copolymers: theory and experiment. Annual Review of Materials Science 26, 501–550.

Garcia, R., 2006. Etude du comportement sous déformation de copolymère à blocs SBS et SBM à morphologie lamellaire. In: Ph.D. Dissertation, Institut National des Sciences Appliquées de Lyon, France.

Geymonat, G., Müller, S., Triantafyllidis, N., 1993. Homogenization of nonlinearly elastic materials, microscopic bifurcation and

macroscopic loss of rank-one convexity. Archive for Rational Mechanics and Analysis 122, 231–290.
Gido, S.P., Gunther, J., Thomas, E.L., 1993. Lamellar diblock copolymer grain boundary morphology. 1. Twist boundary characterization. Macromolecules 26, 4506–4520.
Hill, R., 1972. On constitutive macro-variables for heterogeneous solids at finite strain. Proceedings of Royal Society of London A 326, 131–147.
Honeker, C.C., Thomas, E.L., 1996. Impact of morphological orientation in determining mechanical properties in triblock copolymers. Chemistry of Materials 8, 1702–1714.
Hutchinson, J.W., Neale, K.W., 1981. Finite strain J_2 deformation theory. In: Carlson, D.E., Shield, R.T. (Eds.), Proceedings of the IUTAM Symposium on Finite Elasticity. Martinus Nijhoff Publishers, The Hague/Boston/London, pp. 237–247.
Idiart, M.I., Ponte Castañeda, P., 2007. Field statistics in nonlinear composites. I. Theory. Proceedings of Royal Society of London A 463, 183–202.
Joo, W., Soo Park, M., Kon Kim, J., 2006. Block copolymer film with sponge-like nanoporous structure for antireflection coating. Langmuir 22, 7960–7963.
Knowles, J.K., Sternberg, E., 1975. On the ellipticity of the equations of nonlinear elastostatics for a special material. Journal of Elasticity 5, 341–361.
Krumova, M., Henning, S., Michler, G.H., 2006. Chevron morphology in deformed semicrystalline polymers. Philosophical Magazine 86, 1689–1712.
Laws, N., 1973. On the thermostatics of composite materials. Journal of the Mechanics and Physics of Solids 21, 9–17.
Lebensohn, R.A., Tomé, C.N., Ponte Castañeda, P., 2007. Self-consistent modeling of the mechanical behavior of viscoplastic polycrystals incorporating intragranular field fluctuations. Philosophical Magazine 87, 4287–4322.
Lee, B.J., Parks, D.M., Ahzi, S., 1993. Micromechanical modeling of large plastic deformation and texture evolution in semicrystalline polymers. Journal of the Mechanics and Physics of Solids 41, 1651–1687.
Lopez-Pamies, O., 2006. On the effective behavior, microstructure evolution, and macroscopic stability of elastomeric composites. In: Ph.D. Dissertation, University of Pennsylvania, USA.
Lopez-Pamies, O., Ponte Castañeda, P., 2006. On the overall behavior, microstructure evolution, and macroscopic stability in reinforced rubbers at large deformations: II. Application to cylindrical fibers. Journal of the Mechanics and Physics of Solids 54, 831–863.
Lopez-Pamies, O., Garcia, R., Chabert, E., Cavaille, J.Y., Ponte Castañeda, P., 2008. Multiscale modeling of oriented thermoplastic elastomers with lamellar morphology. Journal of the Mechanics and Physics of Solids 56, 3206–3223.
Lopez-Pamies, O., Ponte Castañeda, P., 2009. Microstructure evolution in hyperelastic laminates and implications for overall behavior and macroscopic stability. Mechanics and Materials 41, 364–374.
Lopez-Pamies, O., Idiart, M.I., 2009. Fiber-reinforced hyperelastic solids: a realizable homogenization constitutive theory (Under revision).
Michel, J.C., Lopez-Pamies, O., Ponte Castañeda, P., Triantafyllidis, N., 2007. Microscopic and macroscopic instabilities in finitely strained porous elastomers. Journal of the Mechanics and Physics of Solids 55, 900–938.
Milton, G.W., 2002. The theory of composites. Cambridge Monographs on Applied and Computational Mathematics, vol. 6. Cambridge University Press, Cambridge.
Nikolov, S., Lebensohn, R.A., Raabe, D., 2006. Self-consistent modeling of large plastic deformation, texture and morphology evolution in semi-crystalline polymers. Journal of the Mechanics and Physics of Solids 54, 1350–1375.
Ponte Castañeda, P., 1996. Exact second-order estimates for the effective mechanical properties of nonlinear composite materials. Journal of the Mechanics and Physics of Solids 44, 827–862.
Ponte Castañeda, P., Tiberio, E., 2000. A second-order homogenization method in finite elasticity and applications to black filled elastomers. Journal of the Mechanics and Physics of Solids 48, 1389–1411.
Ponte Castañeda, P., Willis, J.R., 1999. Variational second-order estimates for nonlinear composites. Proceedings of the Royal Society of London A 455, 1799–1812.
Read, D.J., Duckett, R.A., Sweeney, J., McLeish, T.C.B., 1999. The chevron folding instability in thermoplastic elastomers and other layered materials. Journal of Physics D 32, 2087–2099.
Séguéla, R., Prud'homme, J., 1981. Deformation mechanism of thermoplastic 2-phase elastomer of lamellar morphology having a high volume fraction of the rubbery microphase. Macromolecules 14, 197–202.
Triantafyllidis, N., Maker, B.N., 1985. On the comparison between microscopic and macroscopic instability mechanisms in a class of fiber-reinforced composites. Journal of Applied Mechanics 52, 794–800.
Triantafyllidis, N., Nestorvić, N., 2005. Onset of failure in finitely strained layered composites subjected to combined normal and shear strain. Journal of the Mechanics and Physics of Solids 52, 941–974.
Tzianetopoulou, T., 2007. Micro- and macromechanics of single crystal and polygranular lamellar block copolymers. In: Ph.D. Dissertation, Massachusetts Institute of Technology, USA.
Tzianetopoulou, T., Boyce, M.C., 2004. Micromechanics of PS/PB/PS triblock-copolymer films with lamellar morphology. Materials Research Society Symposium Proceedings 788, L9.3.
Vogler, T.J., Hsu, S.-Y., Kyriakides, S., 2001. On the initiation and growth of kink bands in fiber composite. Part II: analysis. International Journal of Solids and Structures 38, 2653–2682.
Willis, J.R., 1977. Bounds and self-consistent estimates for the overall properties of anisotropic composites. Journal of Mechanics and Physics and Solids 25, 185–202.
Willis, J.R., 1981. Variational and related methods for the overall properties of composites. Advances in Applied Mechanics 21, 1–78.
Yang, S.Y., Ryu, I., Kim, H.Y., Kim, J.K., Jang, S.K., Russell, T.P., 2006. Nanoporous membranes with ultrahigh selectivity and flux for the filtration of viruses. Advanced materials 18, 709–712.